FINAL REPORT

Contract Number: *DTPH56-14-H-CAAP02*

Prepared for: *DOT*

Project Title: *Wall Break-through in Composite Repaired Defects*

Prepared by: *The University of Tulsa*

Contact Information: *Michael W. Keller, mwkeller@utulsa.edu*

Executive Summary

Pipework and pressure vessels are subject to environmental degradation due to corrosion, erosion, and external actors. This damage acts to reduce the wall thickness of the vessel or introduce other stress concentrations that threaten the structural integrity of the equipment. Repair of damaged piping and pressure vessels has traditionally been accomplished using welded repairs, where a patch material is attached to the substrate over the damage. During the past two decades, the use of composite materials to repair damaged pipelines has experienced a considerable increase as these repairs have become more cost effective and efficient. These repairs are frequently installed on damage generated by corrosion or erosion that begins as a wall-loss defect that can transition to a through-wall defect. Critically, the damage generated by the process tends to have a region of diffuse wall loss surrounding a through-wall penetration. Design qualification of repairs for through-wall defects are performed using simulated flaws manufactured by drilling through the pipe wall. This creates straight-sided flaws with significant remaining stiffness, very different from the diffuse, tapered flaws produced by erosion or corrosion. This study will investigate the performance of composite repairs installed on drilled defects and diffuse flaws generated by an erosion process. Two different geometries, a 6 in diameter straight vessel and a 4 in diameter long radius elbow, are studied in this work. Finite element analysis is performed to help understand the influence of the shape and size of the damaged region on repair performance. Hydrostatic pressure testing of damaged and repaired test specimens is performed and the failure pressures of repairs installed on drilled and diffuse flaws are compared. Digital image correlation is performed to understand the

development of strains in the repair and to provide a quantitative comparison between the two flaw types.

Based on the results of this study, symmetric regions of diffuse damage did not appear to significantly impact the performance of the repair. Failure pressures from diffuse damage specimens and drilled specimens were statistically similar. An increase in pin-hole, or through-repair, failures was observed for thinner repairs with diffuse damage. This indicates that no special considerations are required for repairing these defect types. When the region is significantly asymmetric, such as in the case of erosion damage in elbows, repair performance was statistically different. For asymmetric damage failure pressures were lower than drilled specimens or symmetric damage. However, the use of the axial flaw models in ASME PCC-2 did provide a conservative estimate for repair failure pressure. These suggestions have been provided to the ASME PCC committee for consideration.

1 INTRODUCTION

Carbon steel materials are commonly used in a wide variety of industrial settings. These materials are cost-effective and possess mechanical properties that are attractive for many applications, including structural shapes, pressure equipment and pipelines for oil and gas transportation. Carbon steel pipe is attractive for transportation applications as the material is inexpensive and readily available [1]. One of the downsides of carbon steel is that this material is susceptible to both erosion and corrosion [2]. In many cases, carbon steel elements are in contact with environments that can chemically attack and deteriorate the carbon steel structures. Also, erosion can promote corrosion by removing a protective surface treatment or protective corrosion products [3].

1.1 Damage in Pipelines and Pressure Equipment

As mentioned above, damage in pipelines can come from many sources. Two commons sources of damage are corrosive processes and erosive processes. Central to both of these processes is the production of regions of diffuse damage that can extend for significant distance. For the case of erosion, which is a mechanical wear process, material is slowly removed by repeated deformation and cutting actions caused by solid particle impingement. Erosion has received significant attention amongst researchers in recent years [4–5]. This attention is due to the severity of the problems caused by this phenomenon to components in service, which leads to component degradation and subsequent equipment failure. Much work has been directed towards providing a

fundamental understanding of this complex mode of failure and proposing models and mechanisms that would account for the observed erosion rates [6].

Erosion in transportation pipelines is most likely to happen in transitions and geometry changes. Bends act like concave mirrors and reflect the flow (with any entrained particles) to wear hot spots shown in Figure 1.1. Impacts between particles and bend walls can be at any angle between normal and parallel to the surface. The variation in impact angle can result in multiple erosion mechanisms which lead to cutting, deformation and ploughing wear for bends manufactured from ductile materials [1].

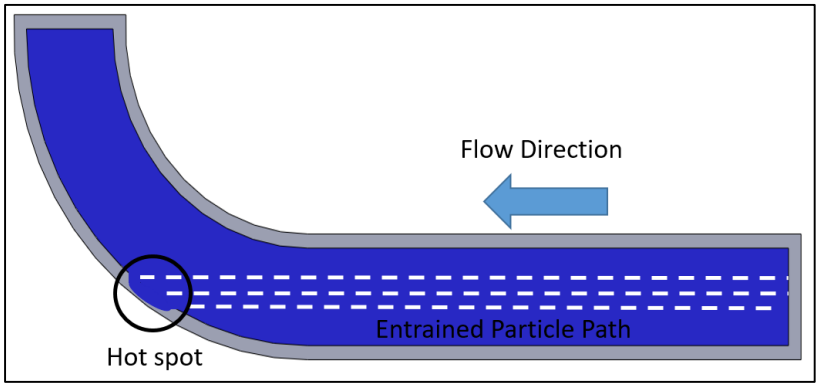

Figure 1.1: Erosion in bends

There are several erosion mechanisms, one of them is erosion by cutting which produces plastic deformation by removing chips by a process of micro-machining. Target melting mechanism occurs when the energy lost after the impact is converted into heat which, when concentrated into a sufficiently small volume, could cause the target material to be melted [7]. Also, there is a combined forging extrusion mechanism which produces small highly distressed platelets of target material that are knocked off the surface by succeeding particle impacts and this mechanism is responsible for erosion at both low and high impingement angles [8].

1.2 Repair of Pipelines and Pressure Equipment

In pressure equipment, erosion or corrosion can occur both internally and externally. In both cases, the subsequent material loss can severely degrade the mechanical integrity of the system and lead to failures. As such, considerable research efforts have been expended to investigate strategies for the mitigation of this damage and the repair of already damaged equipment [9-10]. In a recent survey, it was reported that there is a total of 3.5 million km of pipeline in 120 countries. The United States has approximately 65% of the total pipeline installed in the world. The average annual corrosion-related cost is estimated at $7 billion dollars to monitor, replace, and maintain these pipelines [11].

Traditionally, damaged pressure equipment have been rehabilitated using welded metallic repairs. These are effective, but can be difficult to fabricate for complex shapes. Additionally, metallic repairs can sometimes be challenging to install on operating pressure equipment due to the risk of flammable fluids inside the pipeline such as natural gas. Another method is grinding out the surface of the pipe to produce smooth surface and remove harmful stress concentrations, defects and micro cracks. Afterwards, the surface is recoating with a protective epoxy coating. Some disadvantages for this method are that it cannot be applied to through-wall defects and the operating pressure should be reduced to 80 percent during the repair process [12]. Finally, there is the option to replace the pipe, which is typically the most expensive and time consuming method for pipeline restoration.

1.3 Composite Repairs

Since the 1990's, composite materials have been seen as an alternative to repair and reinforce pressure equipment [13]. Some of the advantages of composite materials are that they are very flexible and can be installed in geometries such as elbows and bends. Also, most composite materials have excellent resistance to corrosion which is a very important parameter within the oil and gas industry. A composite repair is formed from three general components. A reinforcement phase, which is typically a woven reinforcement cloth, a matrix material, epoxy and polyurethanes are common, and a dimensional restoration epoxy, which returns the substrate to the original exterior profile [14]. The reinforcement and the matrix material form the load-bearing, structural repair system. While the dimensional restoration epoxy is used to fill surface defects in the corroded pipe wall to allow for a uniform surface for the over-wrap to be applied. The dimensional restoration epoxy material is the medium through which the internal pipe pressure is transferred to the repair.

Composite wraps work by sharing the hoop stress in the pipe wall so that the MAOP pressure can be safely maintained. The repair, accordingly, offers the advantage of restoring the full strength of damaged pipeline, increasing its stiffness, and inhibiting the external corrosion since the composite acts like an external coating [12].

1.4 Standards for Composite Repairs Design

One of the most significant developments in composite repairs was the development of two, related design codes, ASME PCC-2 [15] and ISO T/S 24817. These standards provide guidance for repair design requirements and provide required testing and

qualification procedures. Both documents classify damage into two broad classes, through-wall defects and non-through wall defects. For the case of non-through-wall defects, the design approach is either stress or strain-based and the ultimate tensile properties of the composite are the critical design parameters. For the case of through-wall defects, the critical material parameter is the interfacial fracture behavior of the substrate-composite interface [13]. The starting point for the analysis is a Griffith critera for fracture that uses the change in volume of the repair V due to crack area extension A to define the fracture energy

$$\Gamma = \frac{1}{2} P \frac{\partial V}{\partial A} \tag{1}$$

To apply this relation, a theoretical prediction of the out of plane displacement of the repair is required to calculate the volume change as a function of crack radius. The relationship is taken from plate theory, which considers the repair material as isotropic. The deflection of the plate is given by

$$y(r) = p\left[\frac{3(1-\nu^2)}{16Et^3}(a^2 - r^2)^2 + \frac{3}{8Gt}(a^2 - r^2)\right] \tag{2}$$

Combining this relationship with Equation (1), it can be derived a relationship between composite material properties, defect geometry and applied pressure.

$$\Gamma = p^2\left[\frac{1-\nu^2}{E}\left(\frac{3}{32t^3}a^4 + \frac{2}{\pi}a\right) + \frac{3}{16Gt}a^2\right] \tag{3}$$

Where the modulus E is the sum square of composite axial and hoop modulii, G is the composite shear modulus, ν is the in-plane Poisson ratio, t is the repair thickness, a is the crack extension, and p is the internal pressure. This approach has worked well for design, but has limits when attempting to extend or improve the design equations.

1.5 Goals of the Research Project

Figure 1.2(a) shows the current model flaw geometry, which does not take into consideration that most flaws are not straight sided holes, but have regions of diffuse damage (b). The goal of this research is the comparison of repair performance on drilled and diffuse flaws generated through erosion. This comparison will be done in terms of failure pressure, out of plane displacement and strains at the defect location. To perform this comparison, both defects will be generated and repaired on straight and elbow specimens. Eroded defects will be generated using dry erosion directed to a fixed location until defect becomes through-wall. Performance of the repairs will be assessed using hydrostatic testing to determine the failure pressure for each specimen type. Digital image correlation (DIC) will be performed in the specimen in order to obtain displacements and strains to evaluate the repair response as pressure is gradually increased.

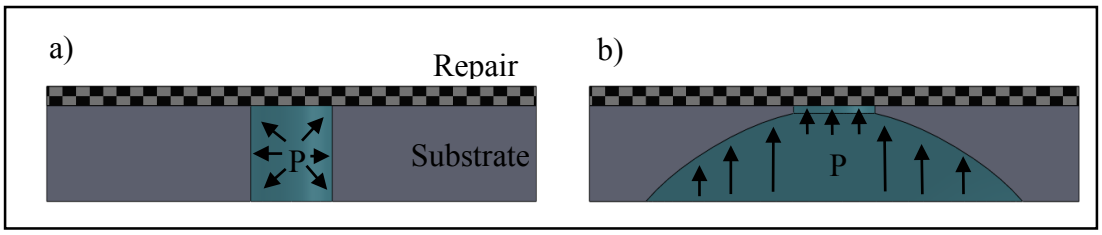

Figure 1.2: Geometries for drilled (a) and eroded defects (b)

2 FINITE ELEMENT ANALYSIS

In this section, FEA simulations and the details of the simulation parameters, material models, boundary conditions and load are described. Results from these simulations are presented with a focus on the tensile opening strains at the interface between the composite and the substrate. Both elbow and straight pipe specimens are included in this study. Flaw parameters are studied, specifically the performance of straight specimens with varying sizes and shapes of erosion damage.

2.1 FEA Modeling Parameters

This section will describe the parameters and assumptions to run the simulations such as material, load and boundary conditions.

2.1.1 Material model and dimensions

The composite material was modeled as a linear-elastic, orthotropic material with material parameters taken from experimental data [16]. The steel substrate material model was a multi-linear elastic plasticity model calibrated using quasi-static tensile tests performed using coupons cut from representative pipe sections [17]. The dimensions for both straight and elbow specimens simulated corresponded to the experimental dimensions. For straight specimens, a 6 in diameter and 4 ft long pipe was simulated. In the case of elbows, a long radius 4 in diameter elbow with 1.5 ft straight sections welded at both ends was used. The composite layer that was assumed to be perfectly bonded to the substrate. Since both specimens have two axes of symmetry, a quarter model of the specimens was analyzed. Representative models are shown in Figure 2.1 for straight

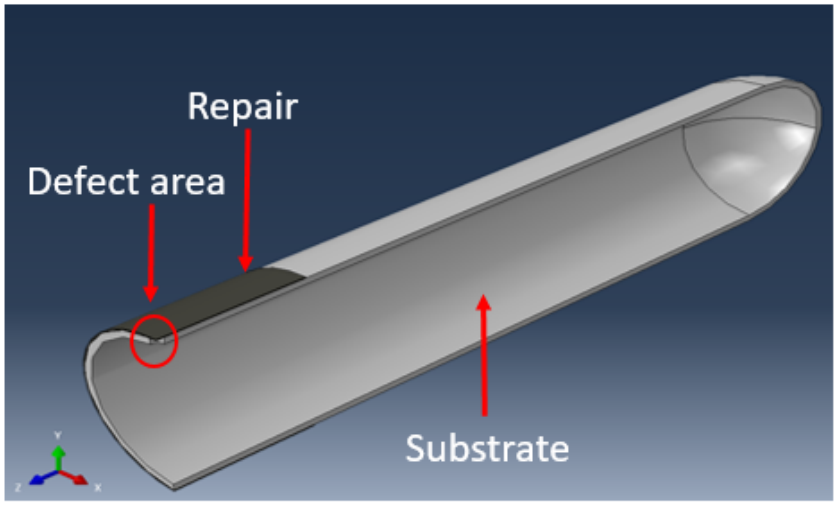

Figure 2.1: Geometry for straight specimens

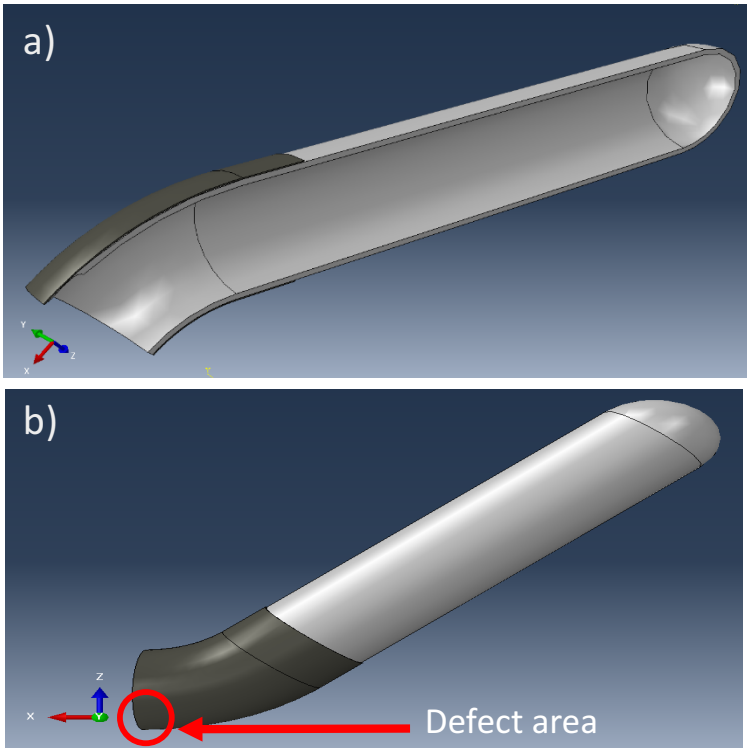

Figure 2.2: Geometry for elbow specimens. Isometric view (a) and top view (b)

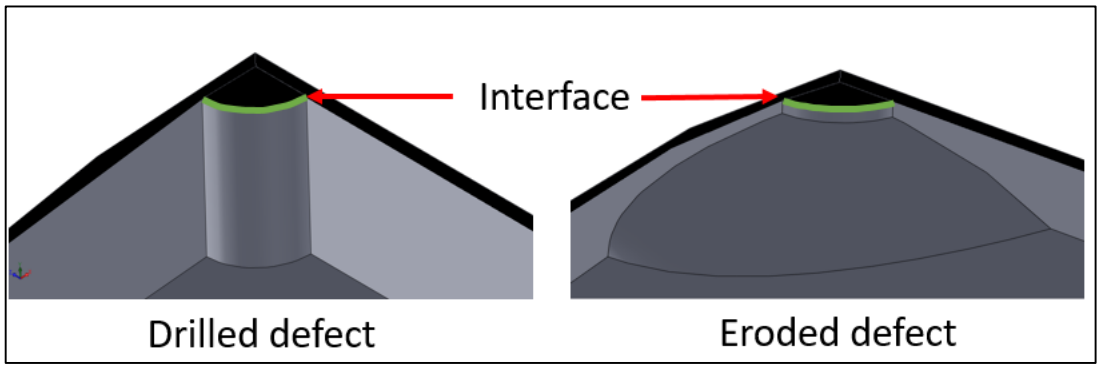

Figure 2.3: Detail in the defects

specimens and Figure 2.2 for elbow specimens. Schematics of the simulated geometry for both types of defects can be seen in Figure 2.3.

2.1.2 Boundary Conditions and Load

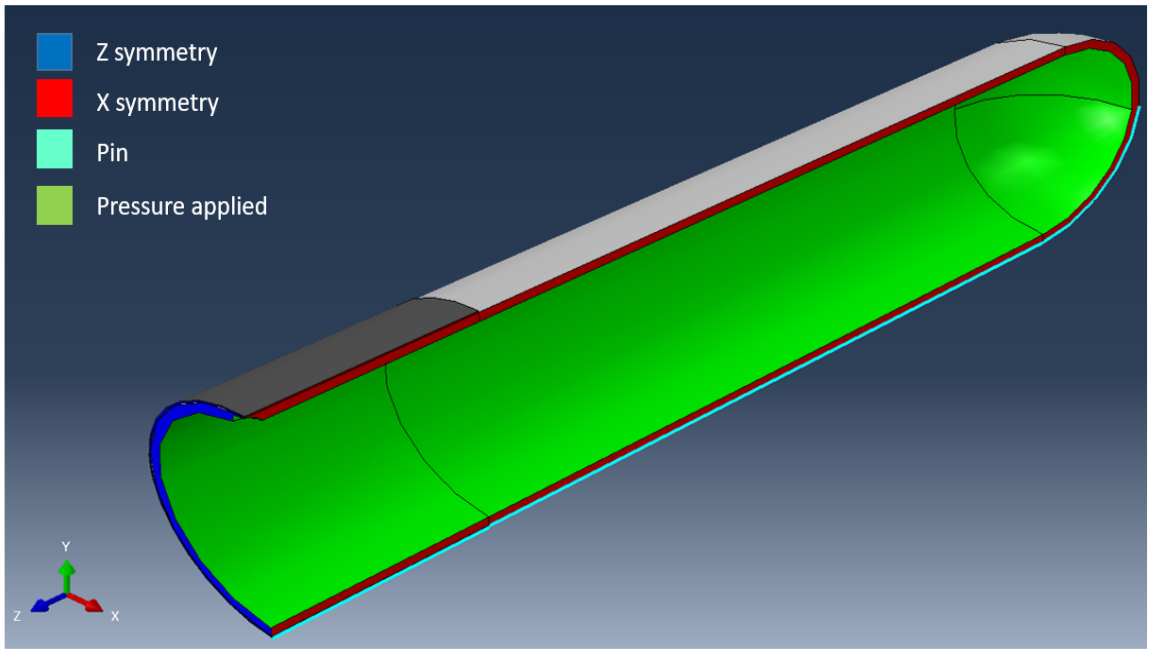

Figure 2.4: Bounday conditions and load for straight pipe

Three boundary conditions were applied to the model. Two edges were modeled with symmetry conditions applied to faces in x and z directions. The bottom edge was pinned to simulate the pipe being attached to the ground. A pressure load was applied to

all internal faces. A schematic representation of the boundary conditions and loading are shown in Figure 2.4.

2.2 Mesh Convergence Study

A mesh convergence study was performed in order to determine a suitable mesh size. For this study, the same element size was applied to the whole system. The mesh was considered converged once the change in maximum stress was less than 1% regardless the element size. An additional convergence study was performed for a model with a local mesh refinement. For this model, the mesh was refined in the area around the hole and a larger general element size applied to the rest of the pipe. An acceptable result was obtained when the refined element size was 0.8 mm and the general size was 3 mm as seen in Figure 2.5.

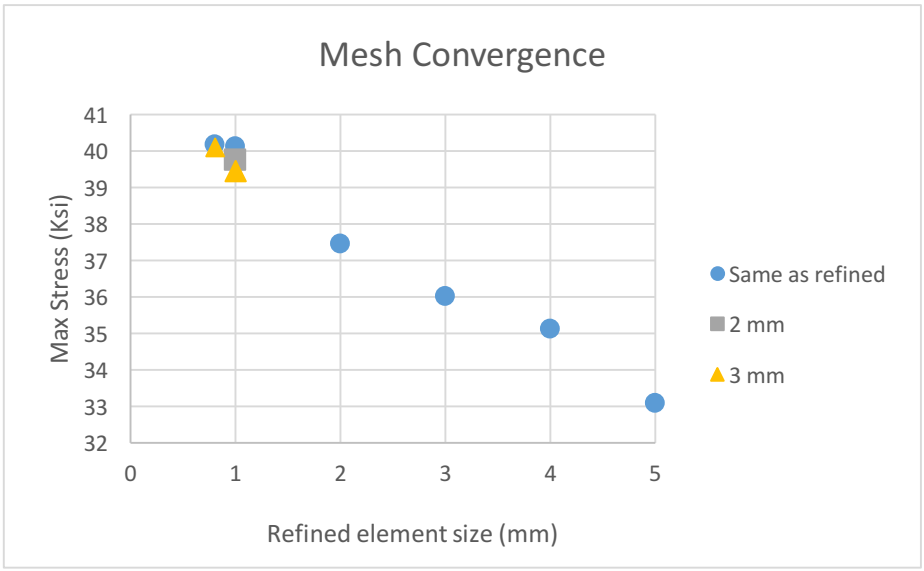

Figure 2.5: Mesh convergence study

2.3 Diffuse Damage in Straight Pipes

Diffuse defects with six different extensions and a drilled defect were simulated to investigate the effect of the size of the diffuse area on the performance of the repair. The diameter of the hole was kept constant and the changing parameter was the diameter of the damaged area. A schematic view of an example defect geometry is illustrated in Figure 2.6 where the defect diameter (e) around the hole is five times the hole diameter (d). Opening strains ε_{22} were obtained at the interface between the repair and the substrate. This interface was of primary interest because it is where the crack is expected to initiate and grow.

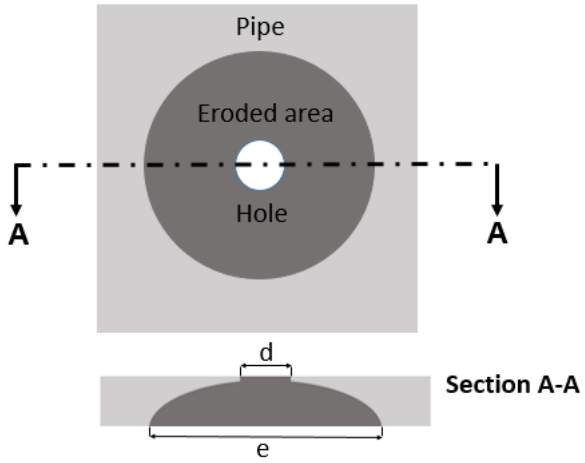

Figure 2.6: Damage size schematic

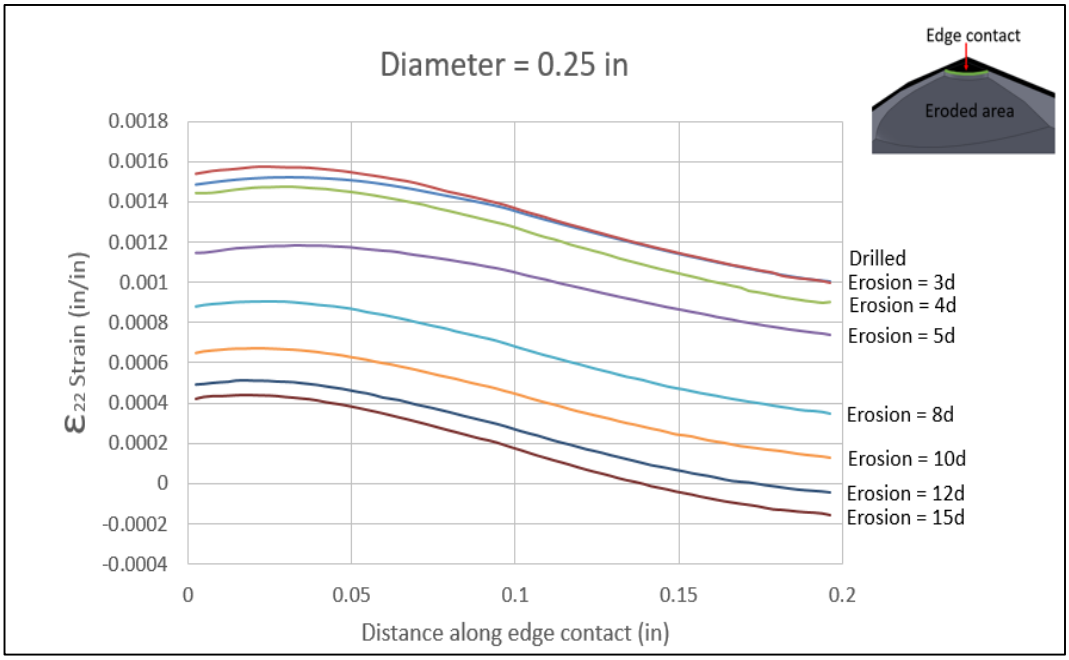

Figure 2.7: Opening strains at the interface for straight pipe with hole diameter = 0.25 in

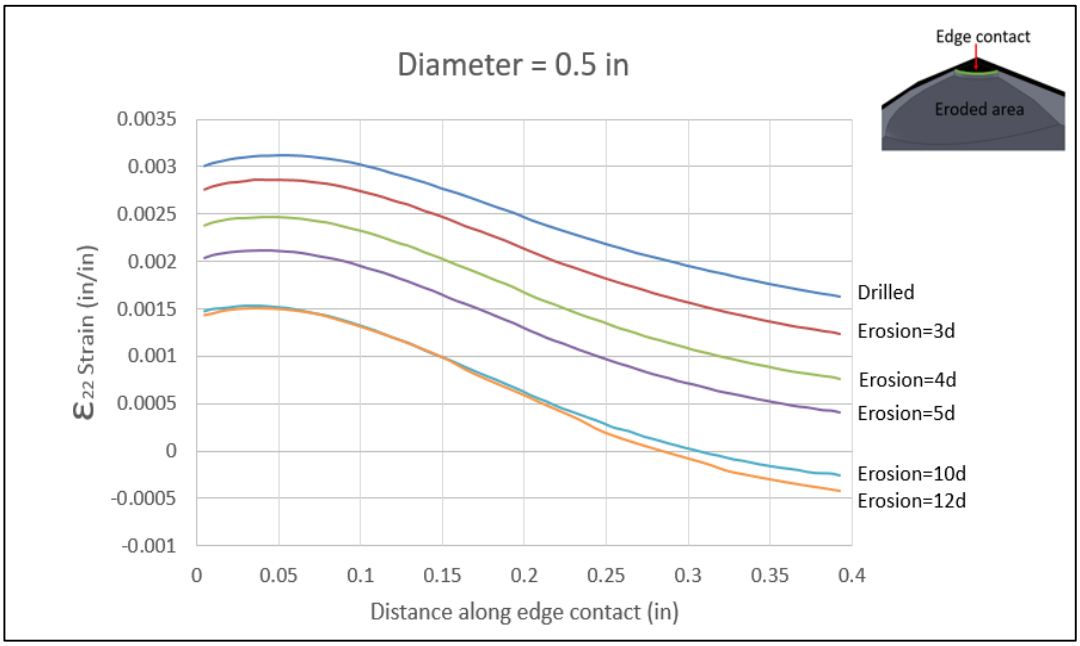

Figure 2.8: Opening strains at the interface for straight pipe with hole diameter = 0.5 in

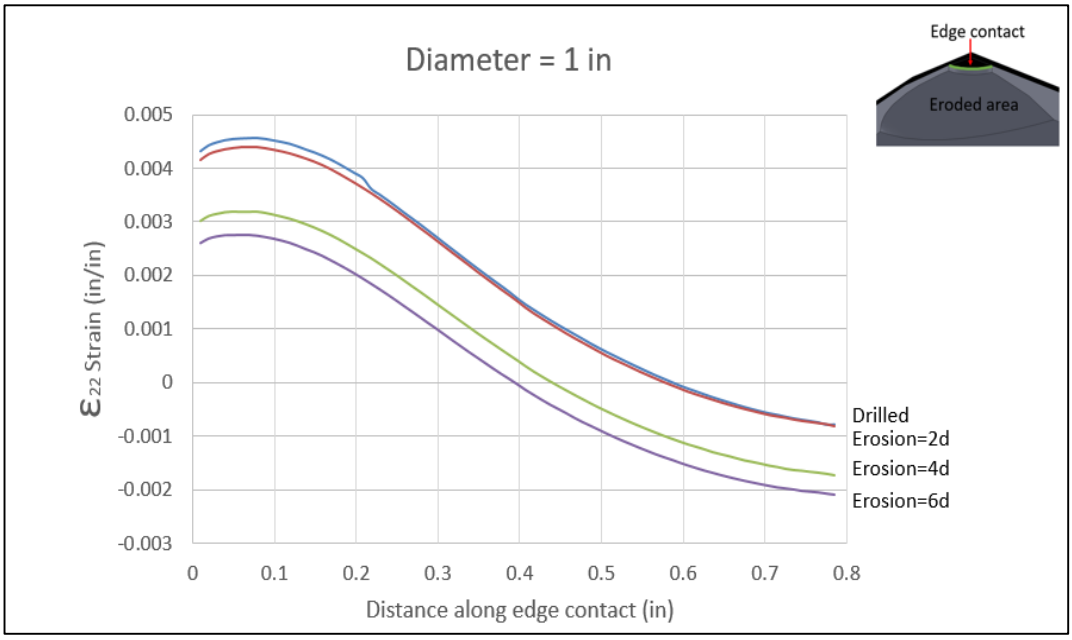

Figure 2.9: Opening strains at the interface for straight pipe with hole diameter = 1in

As seen in Figures 2.7 through 2.9, the trend shows that as the damage area increased, the opening strains decreases. This may be due to the deformation of the thin remaining wall at this location. The applied pressure could be producing additional compression, which would tend to reduce the opening strains. However, there is a non-physical behavior represented by the cusp at the beginning of the contact edge at the symmetry conditions. This behavior is not present in a similar geometry for the elbow specimens presented later and could be caused by the boundary conditions defined in the model. Additional studies are being performed to determine the cause of this behavior. After the diameter of the eroded area approaches 10 times the diameter of hole, the strains become insensitive to the size of the erosion. This may indicate that damage that extends far away from the hole does not have any influence on the repair performance.

2.4 Flaw Shape Study for Straight Pipes

In addition to studying the impact of symmetric variation of erosion around the defect site, the effect of the shape of the eroded area was also studied. Figure 2.10 shows the dimensions used in this study. For this case, W was kept constant with a value of 5 times the radius of the hole and the L value of was increased from 1.4 to 9 times the value of W. This study was motivated due to most erosion patterns found in practical applications and literature had an irregular shape, in most cases similar to an ellipse.

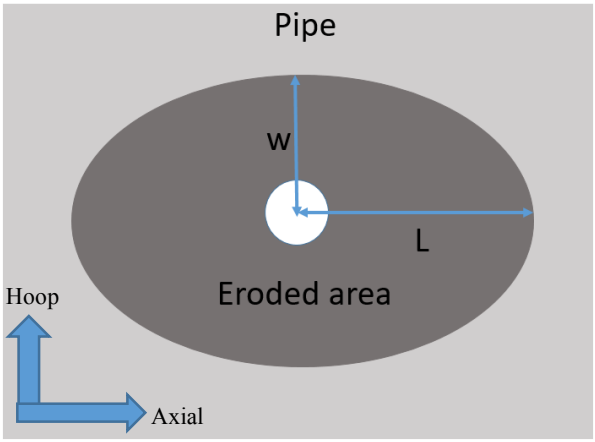

Figure 2.10: Erosion shape scheme

As shown in Figure 2.11, the opening strains increase when this ratio increased. One possible explanation for this behavior is that as the defect becomes longer in the axial direction, the substrate tends to deform in the opposite direction of the repair. The deformation is such that the substrate pulls inward from the outward deflection of the repair, increasing the opening strains. An example of this behavior is shown in Figure 2.12(a) where the pipe is deforming inward while the composite is being pushed outward by the internal pressure. This w shape at the defect location was also obtained experimentally in a pressurized the vessel as shown in Figure 2.12(b). Both the FEA and

the experimental test were performed under the same erosion extent and pressure equal to 700 psi.

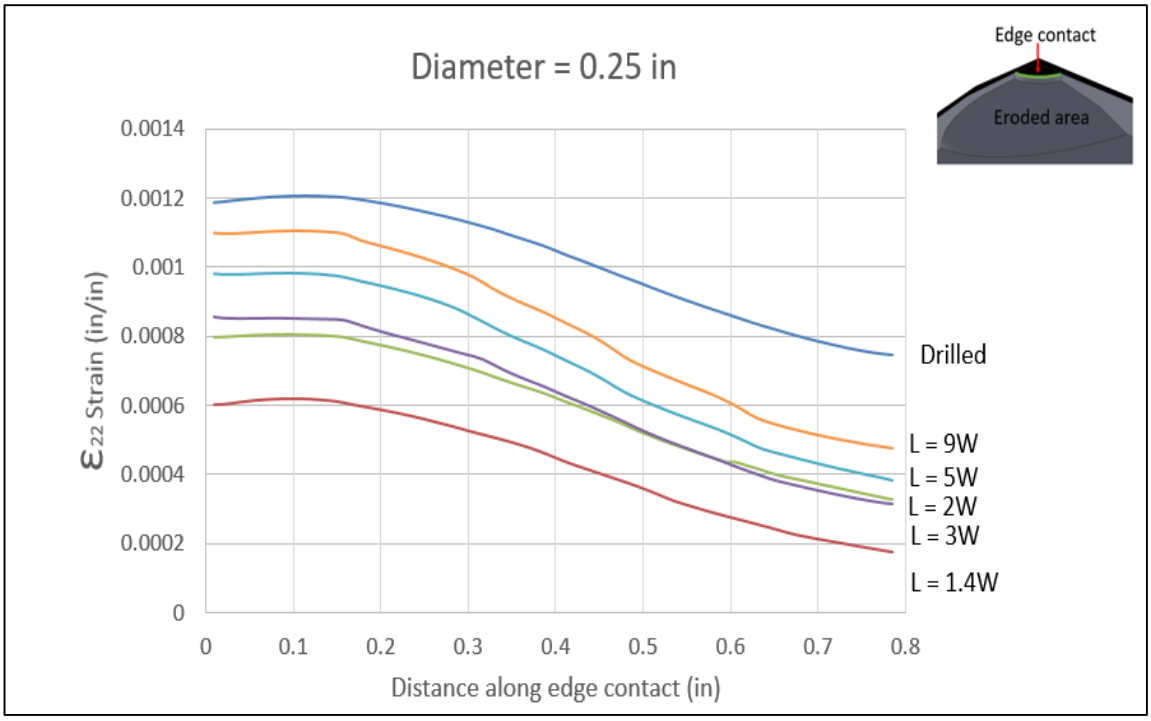

Figure 2.11: Opening strains at the interface for straigh pipe with a hole diameter= 0.25" for shape study

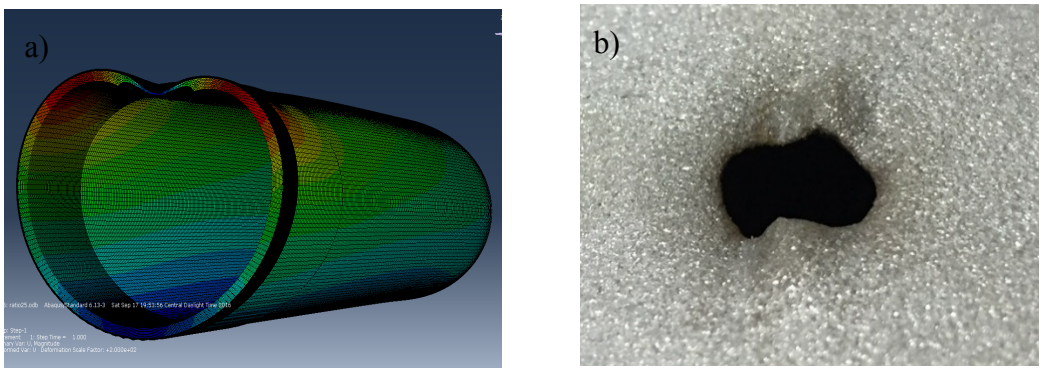

Figure 2.12: Comparison of FEA (a) and experimental results (b) for straight pipe

2.5 Opening Strains for Elbow Assemblies

Opening strains were obtained along the interface between the repair and the substrate. The through-wall defect had a 6.35 mm (0.25 in) diameter at the outer surface of the pipe. In the case of the eroded defect, the damaged area modeled was an ellipse, with the eroded area extending 48 mm in the axial direction and 24 mm in the hoop direction. An ellipse was selected since in most real cases, erosion in elbows takes an elliptical shape [18-19]. A four-layer composite repair was simulated with a total thickness of 1.57 mm. For the analysis presented below, the internal pressure in the elbow was 1000 psi. Similar boundary conditions as used for straight pipes were applied.

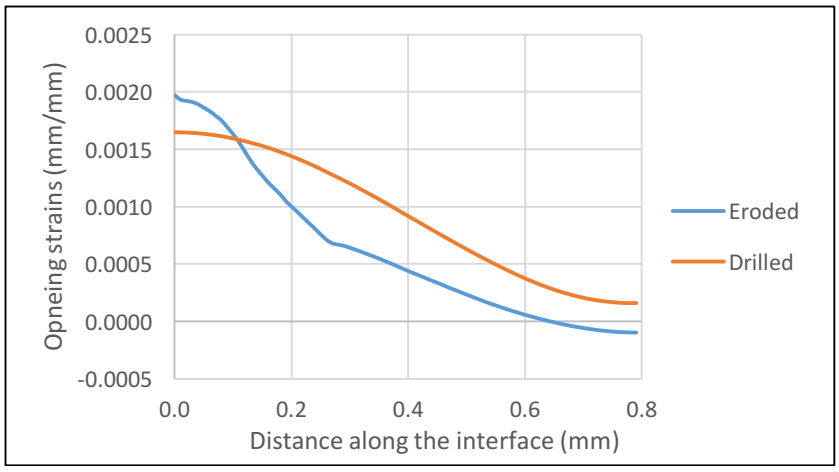

Figure 2.13: Opening strains for elbow assemblies

Figure 2.13 shows the difference in strains for both defects. For the case studied here, the strains were higher for eroded defects in the critical section of the interface as shown in Figure 2.14(a). These higher strains are likely the result of substrate deflection in the opposite direction than the repair in that section of the interface. However, in the rest of the interface, strains are higher for the drilled defects. These higher strains for drilled defects in the non-critical section of the interface are probably due to thin wall deformation in the same direction of the repair as shown in Figure 2.14(b). As will be discussed below,

the higher strains in the critical segment of the interface observed in the simulations were correlated with lower failure pressures in the experiments for eroded flaws.

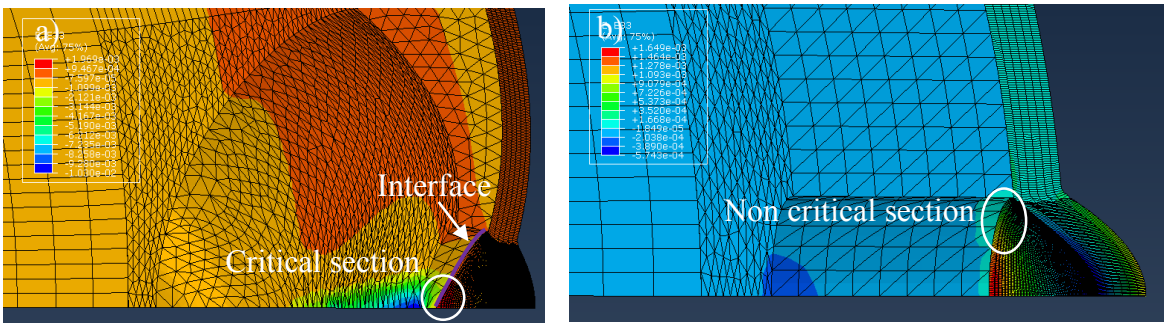

Figure 2.14 Strains at the interface for eroded and drilled defects in elbows

3 EXPERIMENTAL METHODS

In order to compare eroded and drilled defects, test specimens were fabricated with both drilled and eroded flaws. This chapter describes how these defects were created and characterized. Also, specimen assembly, preparation, repairing and testing will be described.

3.1 Material and Geometry for Tests Specimens

In this work, two different geometries were used, a straight specimen and a long radius elbow specimen. For both specimens, the material used was carbon steel ASTM A106b SHC 40 with a specified minimum yield strength (SYMS) equal to 42,000 psi and a wall thickness of 0.28 in. Dimensions and quantities for those specimens are shown in Figure 3.1 and Table 3.1, respectively.

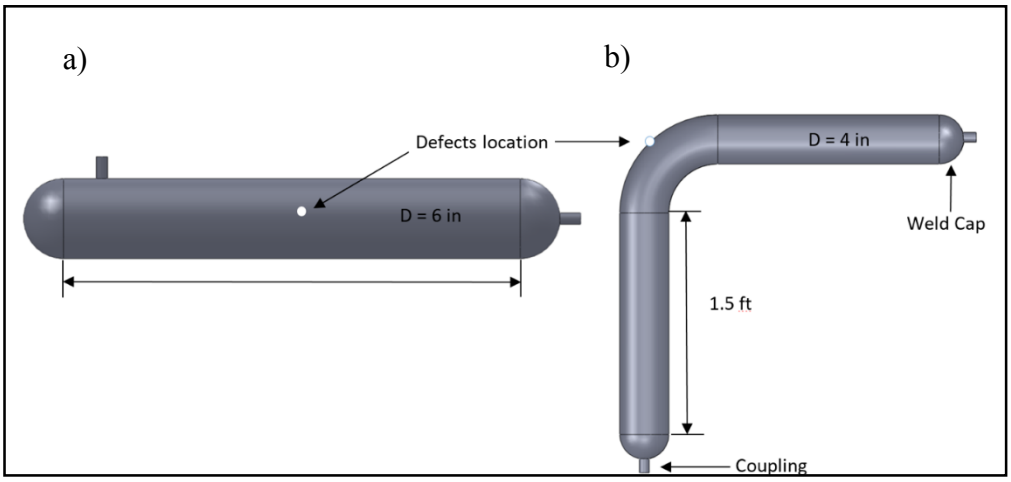

Figure 3.1: Assembly geometry for straight specimens (a) and elbows (b)

Table 3.1: Total number of assemblies created

Assembly	Defect	
	Drilled	Eroded
Straight	2	5
Elbow	2	4

3.2 Simulated Diffuse Flaw Generation

In order to rapidly and repeatedly generate diffuse damaged regions, a gas-driver erosion process was chosen to introduce the defects. This allowed for the formation of defects in a few hours with reasonable reproducibility.

3.2.1 Blast Media Selection

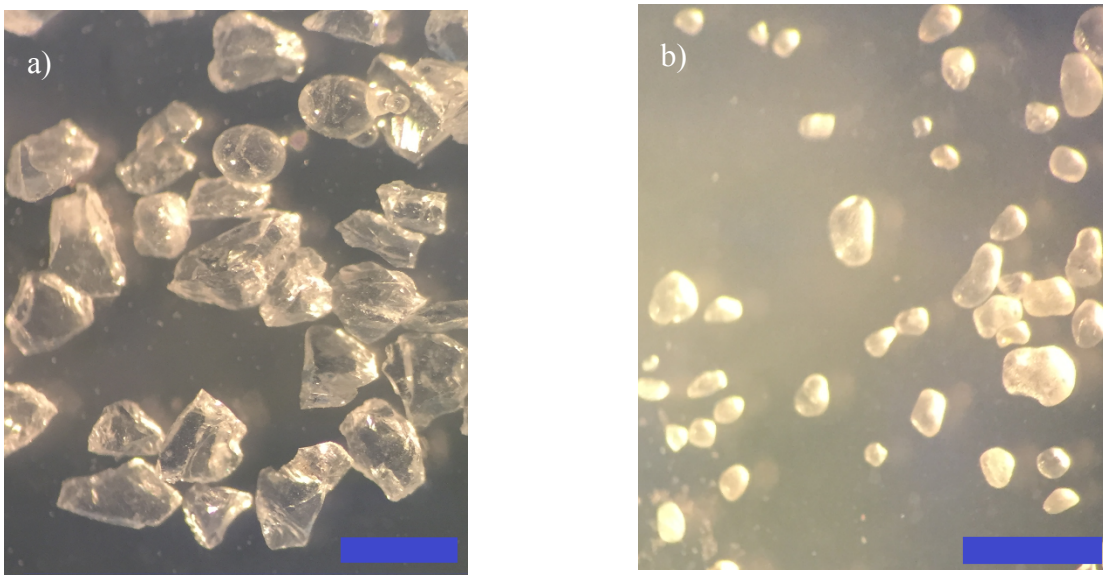

Figure 3.2: Ground glass (a) and sand (b)

Local concentration of force is a function of the geometry of particles. Angular particles with sharp edges can concentrate this force more effectively than rounded

particles. The difference in shape between angular and rounded particles causes a resulting greater difference in erosivity [20]. Since the objective was to create the erosion process as fast as possible, ground glass was chosen as the erodent. As Figure 3.2 shows, ground glass (a) has more angular shape than sand used for this study (b).

3.2.2 Flaw Generation in Straight Specimen

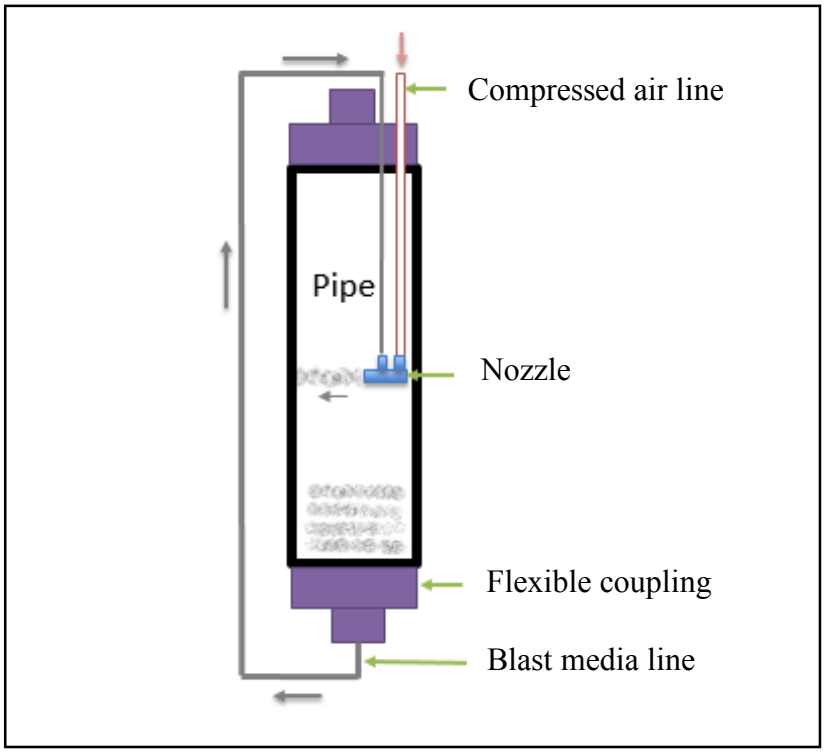

Figure 3.3: Schematic to create erosion on striaght specimen

A diffuse flaw was generated using dry erosion. Since the sample was too long to fit in a commercial blast cabinet, a facility was built to produce the erosion in the pipe. A custom-built nozzle was designed to achieve high particle velocity (in the range of 30 m/s) to ensure that the erosion process was completed in a reasonable amount of time. The time between the initiation of erosion to wall-break through was approximately eight hours. Dry compressed air was used as the gas stream. Flexible couplings at the top and the bottom

sealed the pipe, so the blast media could be re-circulated giving a closed loop erosion system. Flaws were produced by eroding in a specific location until a through-wall defect of approximately 0.25 in was formed. The eroded area produced by this method was similar to a circle. The location of this defect was in the middle of the pipe length to reduce the effect of the end caps on the loading. Figure 3.3 shows the schematic for the set-up.

In addition to the particle erosion method, simulated erosion was performed in two straight specimens using a grinding disk. This method was used because creating an elliptical shape with the previous method was very difficult since the size of the erosion was limited by the distance between the nozzle and the pipe. Using erosion by grinding, a defect with elliptical shape was obtained with an extension of 70 mm in the axial direction and 35 mm in the hoop direction.

3.2.3 Flaw Generation in Elbow Specimen

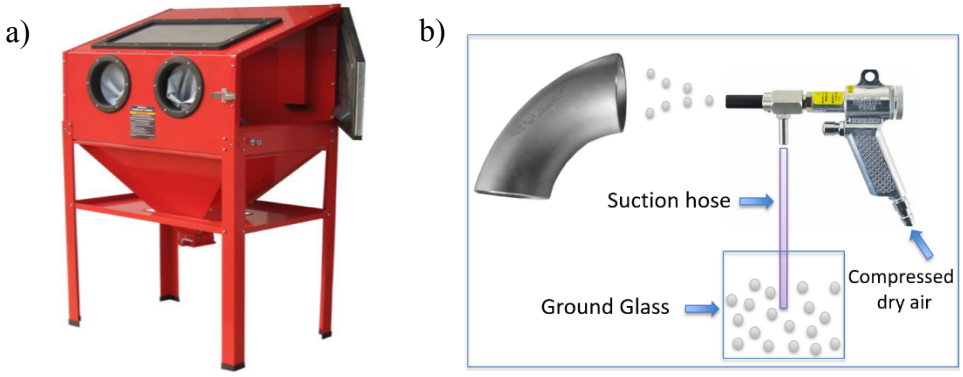

Figure 3.4: Blast cabinet (a) and schematic for nozzle inside the cabinet (b)

Since the elbows were physically smaller, the erosion was performed inside a commercial blast cabinet as shown in Figure 3.4(a). As in the case of the erosion for straight pipes, the blast media was ground glass and dry compressed air was the gas stream. Inside the cabinet there was a nozzle connected to a compressed air line. Both the nozzle and the

elbow were fixed to ensure erosion occurred in the same spot, and the distance between the tip of the nozzle and the impact zone was fixed at 7 inches (b). Since this was a closed cabinet, the blast media fell back into the reservoir after impacting the elbow and could be recirculated. The location of the defect was centered in the elbow as shown in Figure 3.5. This location was chosen based on previous experience with defects from the field.

Figure 3.5: Defect location in elbows

All defects, for both drilled and eroded flaws, had a 0.25 in diameter through-wall penetration. In the case of straight pipes having through-wall defects of 0.5 in diameter, a teflon sticker was placed on the top of the 0.25 in through-wall hole for both eroded and drilled defects. This is equivalent of having a 0.5 in through-wall defect because the teflon prevents the repair from adhering to the substrate.

3.3 Flaw Characterization

3.3.1 Flaw Characterization on Straight Pipe

Since the flaw was generated inside the pipe, direct access for measuring the defect geometry was difficult. To assess the shape and extent of the erosion, an epoxy mold was

made of the flaw to allow for characterization via 3D profilometry. To fabricate this mold, the area near the through-hole was sealed using plastic film, and then a liquid epoxy was poured into the flaw and allowed to cure. Figure 3.6 shows the erosion generated inside the straight pipe by ground glass (a) and the mold once it cured (b).

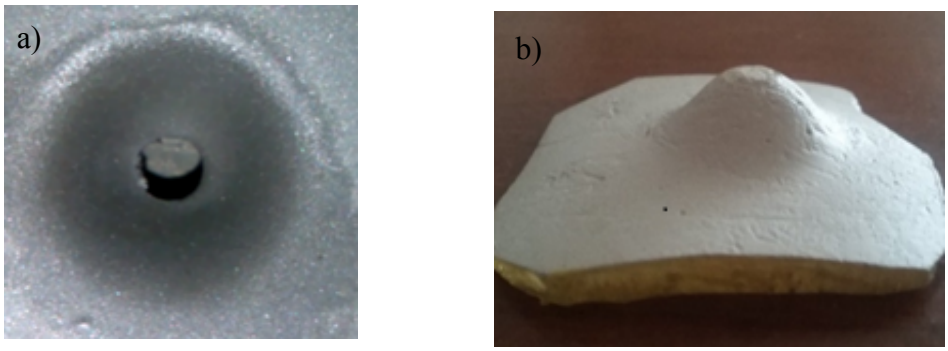

Figure 3.6: Erosion generated inside a straight pipe (a) and defect mold (b)

After curing, this mold was analyzed using optical profilometry. Figure 3.7 shows both the top (a) and the side view (b) of the eroded area. Based on the measurements, the erosion process generated a circular flaw centered around the through-wall penetration. The profile of the erosion area had a tapered and diffuse shape. This confirmed that appropriately shaped flaws were achievable using the erosion process described above.

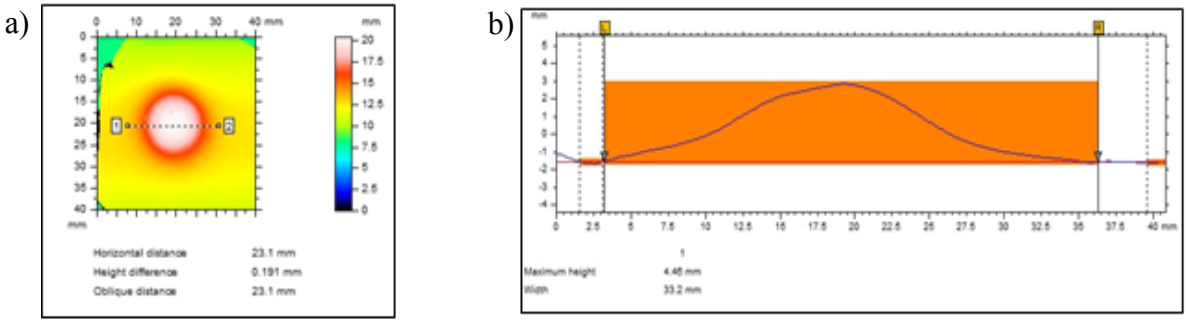

Figure 3.7: Profilometer plots: Top view (a) and side view (b)

3.3.2 *Flaw Characterization on Elbow*

Figure 3.8: Defect mold for elbow specimens

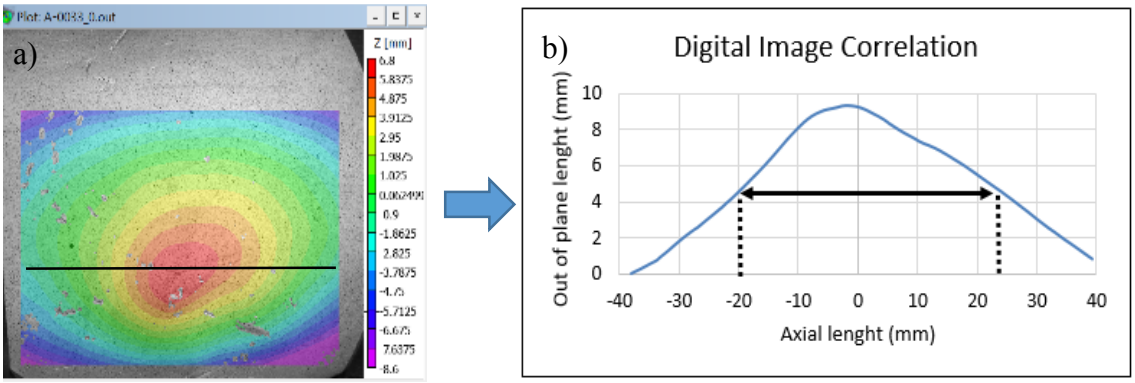

Figure 3.9: Digital image correlation extraction line (a) profile measurement (b)

For elbows, the molding process had to be modified since the defect was located on a curved surface and there was a very smooth transition to the eroded area. This generated a flaw that exceeded the measurement capabilities of the profilometer. Digital image correlation (DIC) was chosen to perform shape measurement on the mold. This method will be described later in this chapter. This mold was bigger than the straight ones in order to be able to detect the small change in slope which indicated where erosion starts.

Figure 3.8 shows the mold, which was made with clay. Figure 3.9 shows the line from which the measurement was extracted (a) and the results (b). From the results, a little change in slope which indicates where the erosion initiates can be seen. Based on this measurement, the eroded area is an ellipse with dimensions of 48 mm along the axial direction and 24 mm in the hoop direction.

3.4 Assembly

Once the defects were completed, two end caps were welded to the straight section of pipe along with two couplings to enable hydrostatic testing. For elbows, two sections of straight pipe were welded to complete the specimen before the addition of end caps and couplings.

3.5 Repair Installation

Prior to installation of the repair, the exterior surface of the substrate was grit-blasted to a NACE 2 finish (near white-metal) which stipulates that when viewed without magnification, the sample shall be free of all visible oil, grease, dust, dirt, mill scale, rust, coating, oxides, corrosion products and other foreign matter of at least 95% of each unit area.

3.5.1 Reinforcement

The composite repair system used in this study was based on a carbon fiber reinforcement with a plain weave structure as shown in Figure 3.10. In plain weave, the bundles are aligned so they form a simple cross-cross pattern. Each hoop thread crosses the axial threads by going over one, then under the next, and so on. For straight pipes, a 6k

x 3k fabric was used, which means it has 6000 fibers in the hoop direction and 3000 fibers in the axial direction for every bundle. This fabric was 10 in wide. For the elbows, a 3k x 3k fabric that was 2 in wide was used.

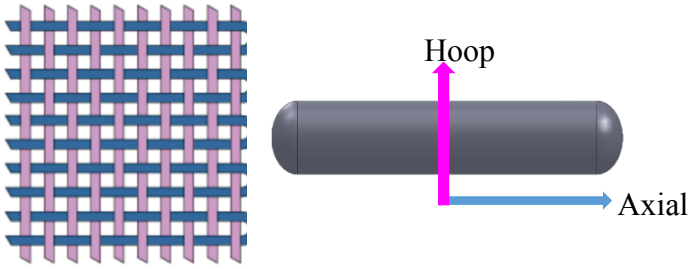

Figure 3.10: Plain wave strcuture of the carbon fiber

3.5.2 Matrix and Primer

The main component for both primer and wet out was Bisphenol A diglycidyl ether (commonly abbreviated BADGE or DGEBA) cured with an aliphatic amine hardener. Primer and matrix have similar chemical compositions in this repair system, but the primer has additives to increase the viscosity of the uncured material.

3.5.3 Installation Procedure for Straight Specimens

Just prior to installation of the composite repair, the substrate is cleaned with isopropyl alcohol to reduce any surface contaminants. The first step of a repair application is to mix and apply the primer as shown in Figure 3.11. Both the resin and the hardener are stirred independently before mixing with each other (a). The primer is applied with a brush and extends approximately two inches from each side of the repair to ensure complete coverage of the area under that repair (b). The repair used was 10 in long, so the total length of applied primer in the axial direction was 14 in.

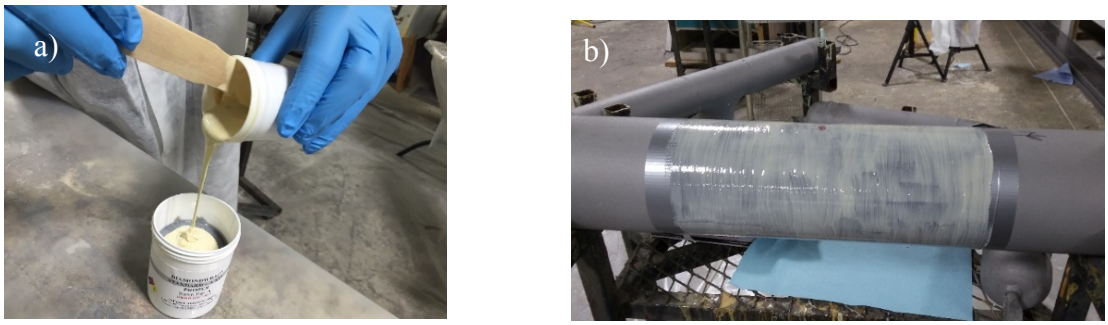

Figure 3.11: Mixing (a) and application of the primer to the substrate (b)

After the primer is applied, the resin and hardener of the wet out epoxy are mixed and applied to the carbon fiber as shown in Figure 3.12(a). In order to saturate the carbon fiber and to avoid any dry spots, a paint roller was used to evenly distribute the epoxy over and through the reinforcement (b).

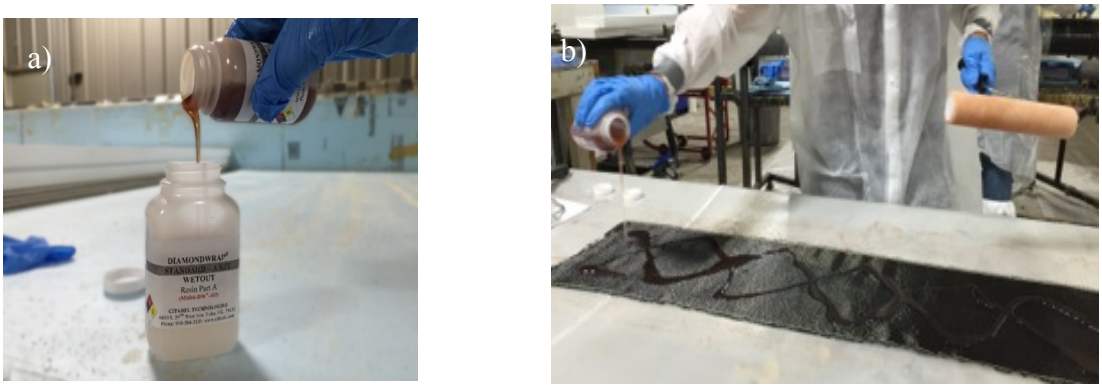

Figure 3.12. Mixing (a) and application of the matrix to the reinforcement (b)

The final step is to roll the carbon fiber into a tube and apply it to the pipe as shown in Figure 3.13(a). The procedure for applying the repair is to wrap the saturated reinforcement around the pipe, with the center of the repair aligned with the center of the

defect (b). During the overwrapping process, a small amount of tension is applied to the composite to ensure that no voids are between the layers of repair.

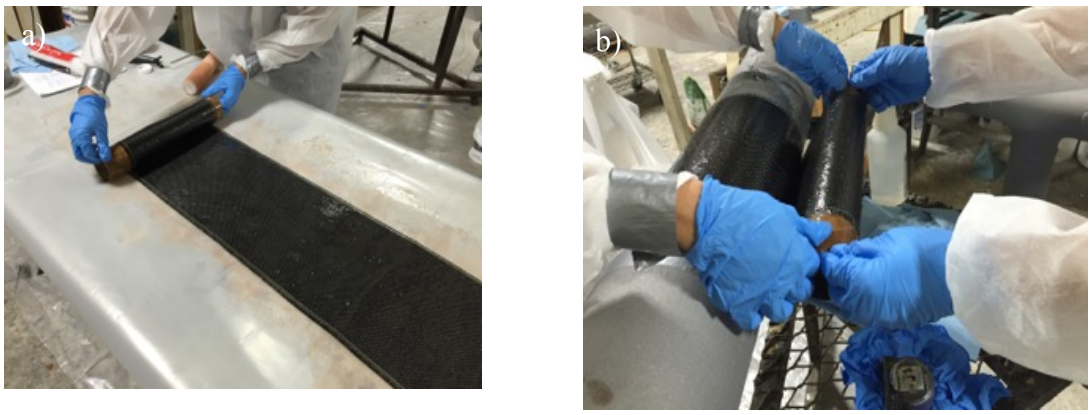

Figure 3.13: Rolling (a) and application of the reinforcement to the substrate (b)

After the composite is installed, the repair is allowed to cure for at least 48 hours at room temperature. Figure 3.14 shows a fully-repaired specimen.

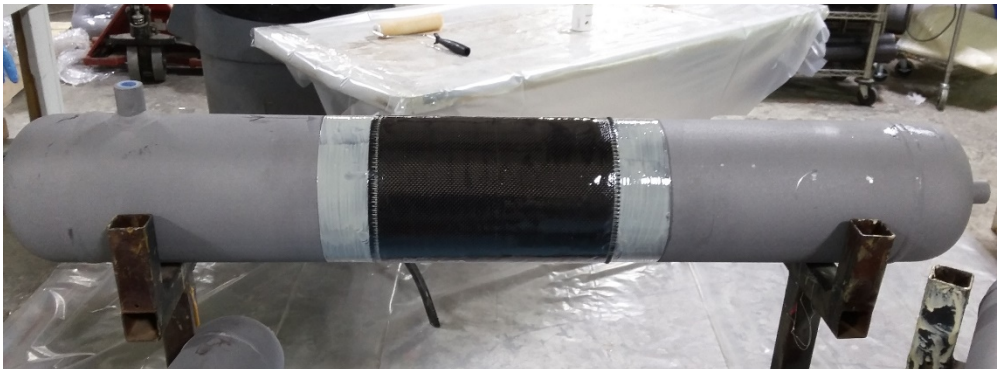

Figure 3.14: Fully repaired substrate

3.5.4 Installation Procedure for Elbow Specimens

The basic installation procedure for elbows is the same as in straight pipes. Because elbows are not a regular shape, the overwrapping procedure is accomplished by a spiral technique. Figure 3.15 depicts the steps in a spiral wrap repair installation. The first step is

to apply a full overlap layer (a) and then start turning by 50% overlap (b) in the centerline until it reaches the other end (c). Each pass provides a two-layer repair. For a four-layer repair, two passes are necessary. Each pass starts from opposite sides.

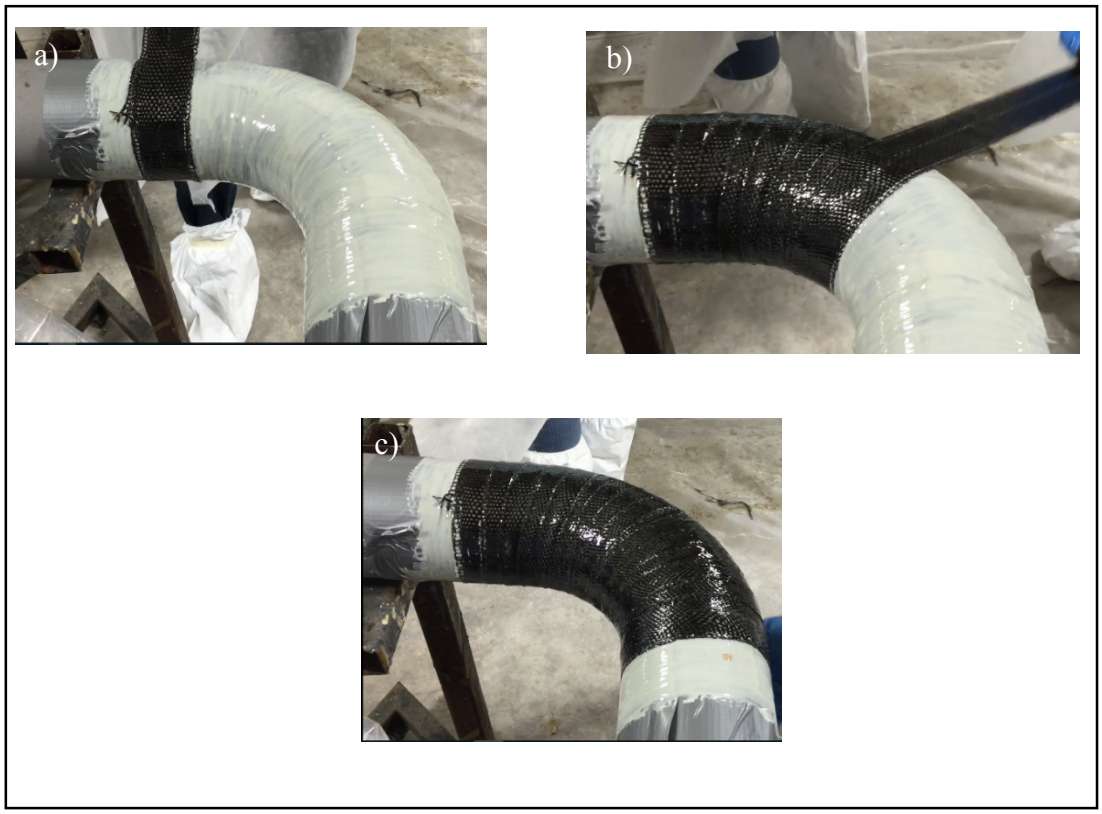

Figure 3.15: Spiral application method

3.6 Hydrostatic Pressure Testing

Burst testing was performed using a hydrostatic pressure test. Test specimens were filled with water and then pressurized until failure using an air driven hydraulic pump (Sprague S216J100) as shown in Figure 3.16. Pressure was applied at a rate of 100 psi every 15 seconds. Once the failure occurred, the maximum pressure was recorded using a digital pressure gage with a memory function. Simultaneous with hydrostatic pressure testing, Digital image correlation was performed on the area around the hole. DIC was used

to investigate both the local strains around the hole and the deformed profile of the repair over the hole. Once failed, specimens could generally be grit-blasted and then used for a new test.

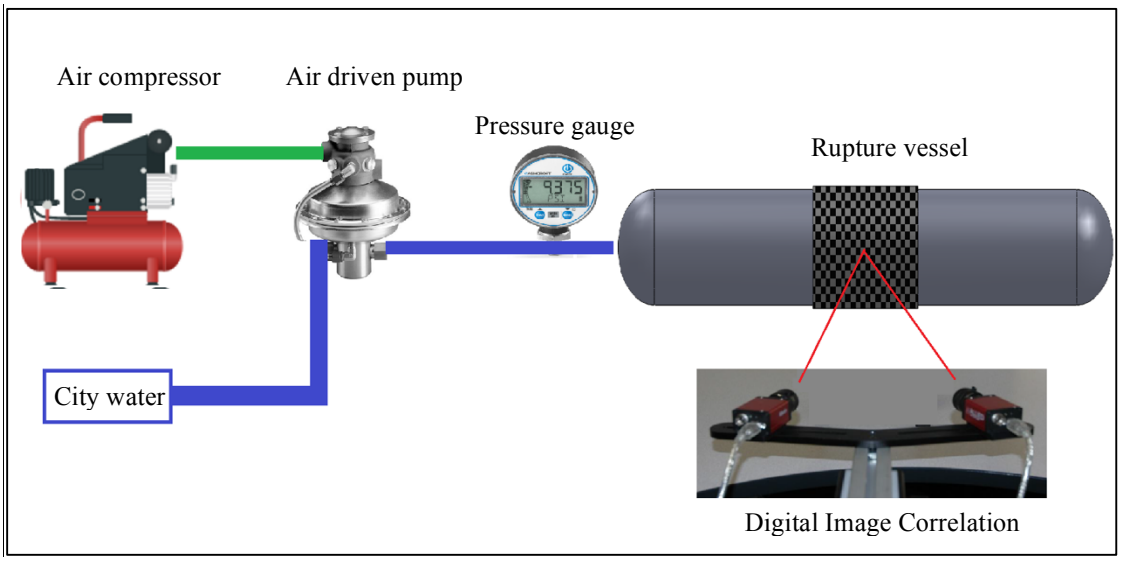

Figure 3.16: Hydrostatic pressure test set-up

3.7 Digital Image Correlation

Digital image correlation (DIC) is a full-field image analysis method widely applied in many areas of science and engineering. This is typically used to measure deformation, displacements and strains. High speed cameras covering the same area are used to capture the change in position of a black and white speckle pattern applied to an object that is under load as shown in Figure 3.17.

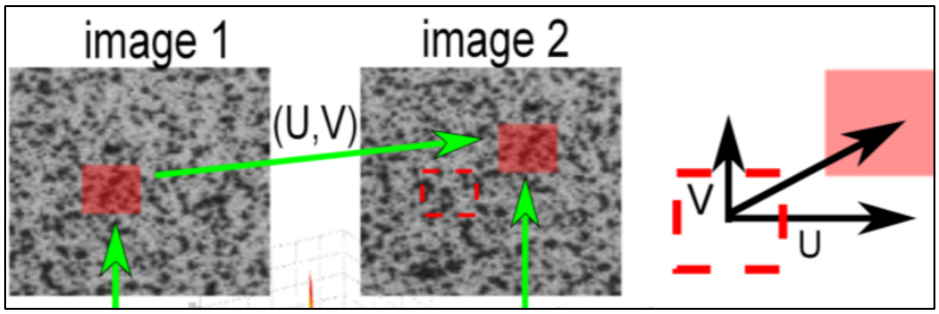

Figure 3.17: Digital image correlation algorithm

Afterwards, a correlation algorithm is run to determine the three-dimensional displacement of a specimen surface as shown in Figure 3.18(a). Based on this, displacements and strains are calculated with the post-processing tool (b).

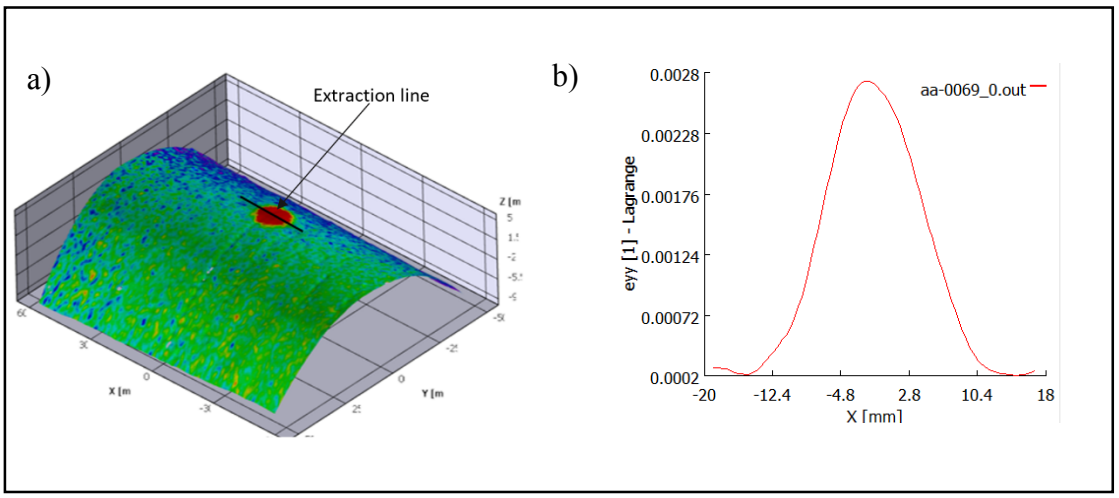

Figure 3.18: Countour (a) and strains obtained by DIC (b)

3.7.1 DIC Procedure

- Create the random pattern over the surface. This is done with spray paint. First, the area is covered with white paint. Once it is dry, a speckle pattern is applied with black paint.
- Place cameras in position: Both cameras must cover the same area and be positioned as symmetrical as possible. These cameras should have an angle

between them at least 15° and below 60° depending on the lenses. The distance is set so that the specimen roughly fills the field of view. In order to have a reference frame, blue tape is applied about 3 inches in every direction. Also, additional lighting is applied over the area to reduce the exposure time of the camera.

- Focus lenses: This is done by increasing the digital zoom in the cameras to about 300%. Focusing is then accomplished using the focusing ring on the imaging lenses.
- Adjust the lighting. The balance between exposure time and lens aperture is adjusted so that the exposure is appropriate for the lighting and the surface. The image cannot be too bright or too dark.
- Calibration: The calibration is performed using an automated algorithm that uses pictures of a calibration grid at different angles and orientations. The grid has to fill approximately the field of view. This procedure uses a bundle-adjustment algorithm to calculate the intrinsic parameters (focal length, principal point, distortion parameter) for each camera and their respective orientation, as well as the extrinsic parameters (translation vector and rotation matrix).
- Data acquisition and analysis: The final step is to take pictures as the load is applied. Once the tests ends, all pictures are analyzed and variables such as displacement and strains can be obtained.

The set-up for the DIC used during testing is shown in Figure 3.19. Cameras are equidistant and with the same angle, additional lighting is in place. The speckle pattern is produced on the surface of the repair in the area near the defect.

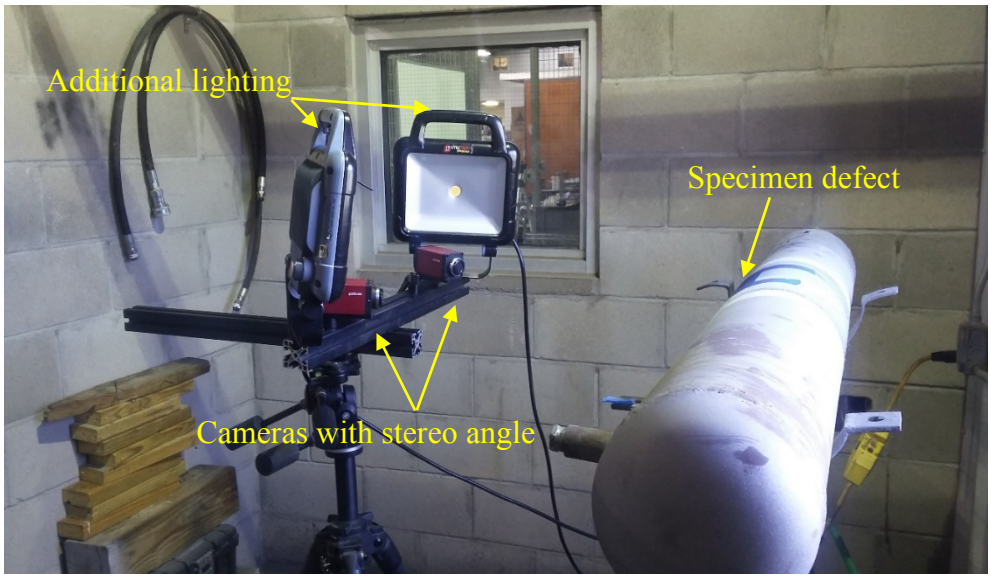

Figure 3.19: DIC set-up

4 EXPERIMENTAL RESULTS

Failure pressure was measured in a total of 30 specimens using different assemblies and ply counts summarized in Table 4.1. Also, Digital image correlation (DIC) was performed on some of those pipes in order to obtain displacements and strains of the repair as pressure was gradually increased.

Table 4.1: Total of assemblies tested

Assembly	Number of layers	Through-wall defect diameter	Drilled	Eroded	Eroded shape
Straight	2	0.25 in	4	9	Circular
Straight	2	0.25 in	-	2	Elliptical
Straight	4	0.50 in	4	3	Circular
Elbow	4	0.25 in	5	4	Elliptical
Total Tests			12	18	

4.1 Hydrostatic Pressure Test

For a test to be considered valid under ASME PCC-2, the failure must be a leak at the edge of the repair. This is because the expression to calculate failure pressure written in this code considers interface failure when the fluid travels through the interface until it reaches the edge, debonding the repair from the substrate. An invalid test takes place when the failure occurs through the wrap. There are several reasons why this happens. One is the presence of voids in the matrix. Another explanation can be that the matrix is not completely cured. Figure 4.1 shows a representation for these types of failures.

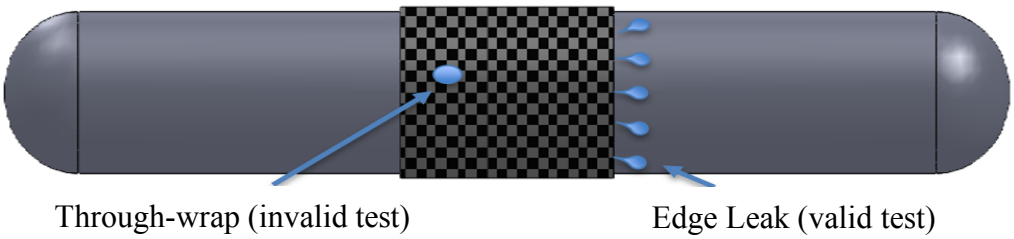

Figure 4.1: Schematic for valid and invalid data points

4.1.1 Straight Assembly with Two-Layer Ply Count

A total of 12 pipes were tested with a two-layer repair on a straight pipe. All pipes had a through-wall defect of 0.25 in diameter. Out of those 12 pipes, 3 had drilled defects and 9 had eroded defects with an eroded area having a circular shape and a diameter about 4 times bigger than the through-wall defect.

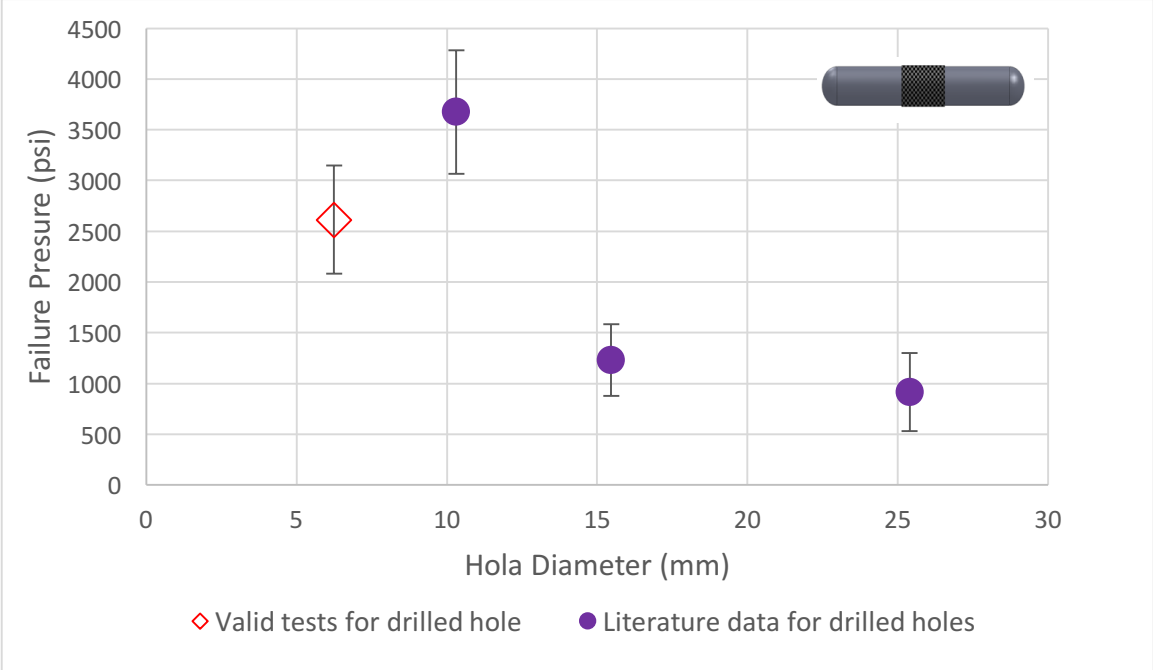

Figure 4.2: Failure pressure for drilled defects with two-layer repair on straight specimens

Figure 4.2 shows a comparison of the test results in the current study compared to previous data obtained on drilled defects. It can be seen that they are below the trend and after running a t-test, they are statistically different with a p value of 0.1083.

Additionally, another two specimens with an eroded defect having elliptical shape with an extension of 11 times the diameter of the through-wall defect in the axial direction and 6 times the diameter of the through-wall defect in the hoop direction were tested in order to evaluate the influence of the erosion shape in the repair performance.

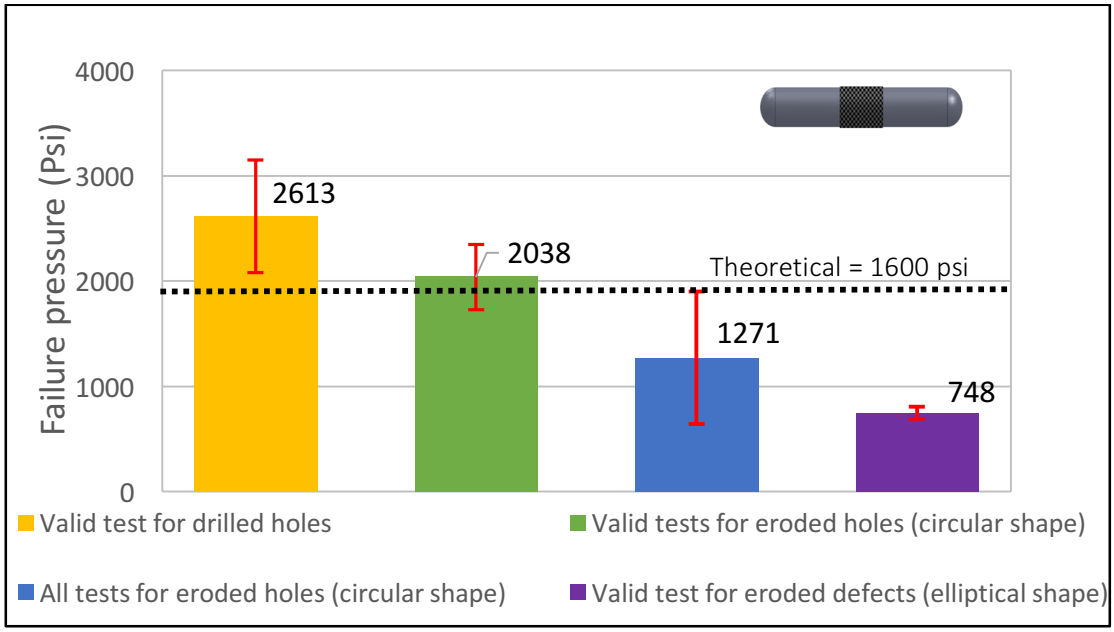

Figure 4.3: Failure pressure for all defects with two-layer repair on straight specimens

Figure 4.3 shows the different failure pressures for all defects. Out of the 9 tests that were performed on specimens with defects having a circular erosion shape, only 3 were valid. This low percentage of valid tests may be due to the fact that the repair was very thin, or as a result of the reduction of the opening strain predicted by FEA. Reducing the opening strains can shift the mode of failure from interfacial failure to bulk composite failure. Comparing the valid tests for eroded defects having a circular shape with the drilled

defects indicated that the failure pressures were statistically different with a p value of 0.279. This result tends to indicate that there is a small variation in fracture energy from eroded to drilled holes. However, both of them are above the theoretical prediction which indicate that the eroded defects do not have a huge impact in the failure pressure for the size of the erosion tested. Comparing all eroded tests regardless of its failure mode, it can be seen that their failure pressures are lower than it would be expected for drilled holes. Finally, comparing the drilled defects with the eroded defects with elliptical shape, it is observed that they are statistically different with a p value of 0.04. Similar to the FEA prediction, the elliptical shape has a significant effect on the failure pressure because the substrate in the region near the through-wall defect is deforming in the opposite direction of the repair, which tends to cause the crack to initiate faster leading to failure.

4.1.2 Straight Assembly with Four-Layer Ply Count

A total of 7 straight-pipe specimens were tested with a four-layer repair. All pipes had a through-wall defect of 0.5 in diameter. Out of those 7 pipes, 4 had drilled defects and 3 had eroded defects with an eroded area having a circular shape and a diameter about 3 times bigger than the through-wall defect.

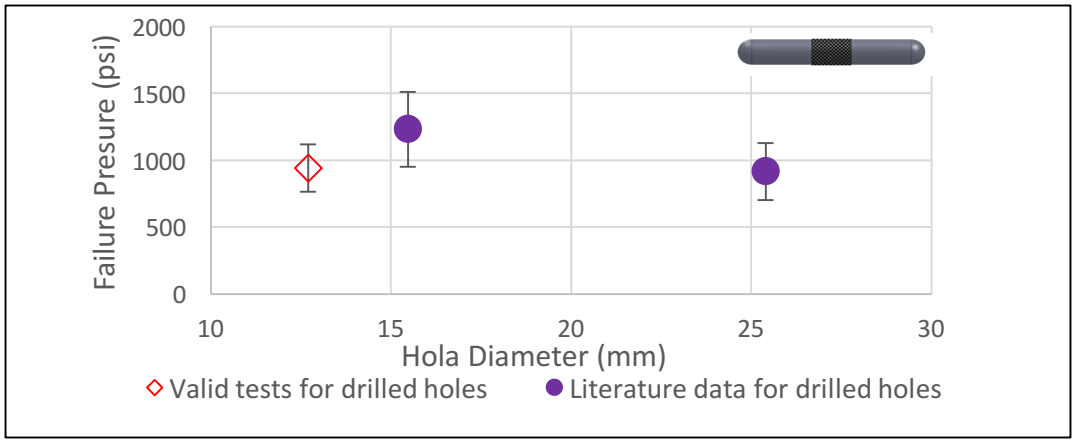

Figure 4.4: Failure pressure for drilled defects with four-layer repair on straight specimens

Figure 4.4 shows the average failure pressure for drilled defects for a four-layer repair. Comparing this failure pressure with experimental data taken from previous work for drilled holes with diameter equal to 15.24 mm, they are statistically different with a p value of 0.1874.

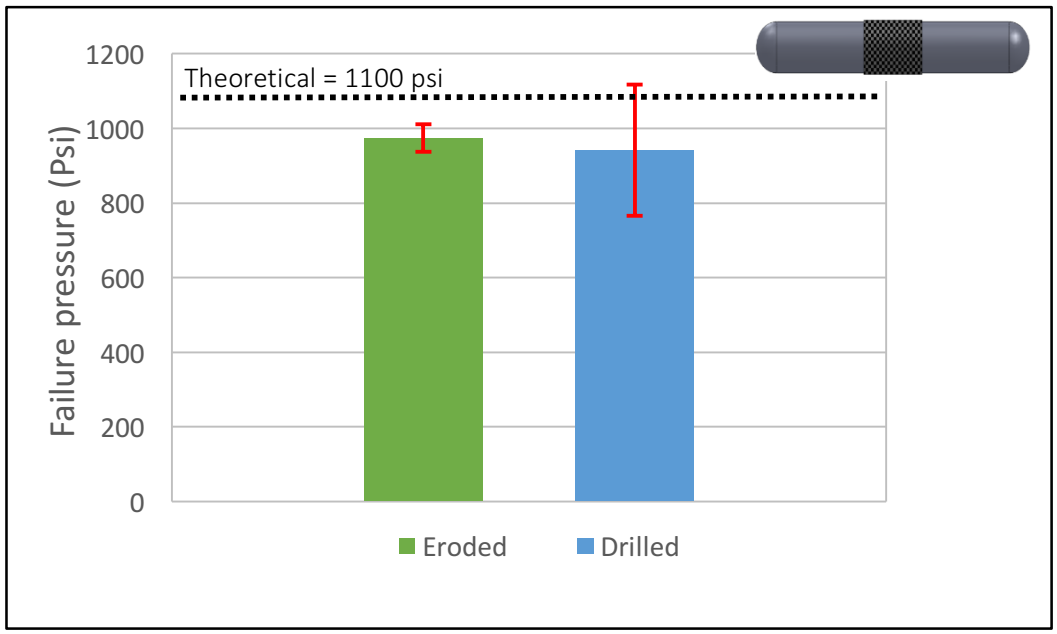

Figure 4.5: Failure pressure for eroded and drilled defects with four-layer repair on straight specimens

In Figure 4.5, it is observed that for this configuration there is not a difference in failure pressure between eroded and drilled defects. Similar to the two-layer repair, this is probably due to the fact that eroded area was not big enough to produce a lower failure pressure in the repair. Also, both defects match very well with the theoretical prediction for this repair thickness.

4.1.3 Elbow Assembly with Four-Layer Ply Count

A total of 9 elbow assemblies were tested with a four layer-repair on elbows. All elbows had a through-wall defect of 0.25 in diameter. Out of those 9 pipes, 4 had drilled defects and 5 had eroded defects with an eroded area having an elliptical shape with an approximate extension of 2 inches in the axial direction and 1 inch in the hoop direction.

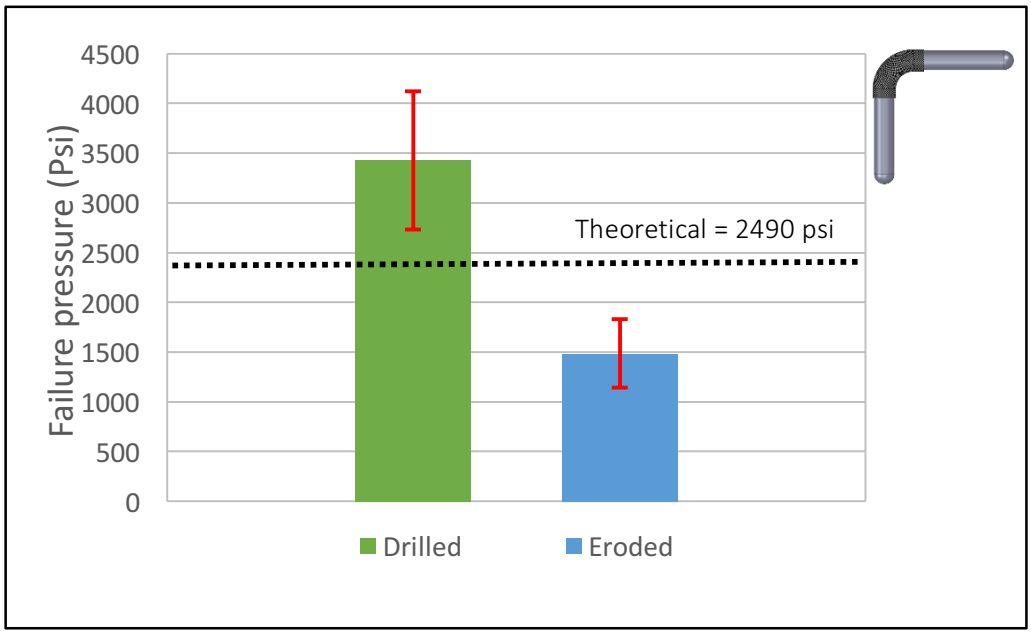

Figure 4.6: Failure pressure for eroded and drilled defects with four-layer repair on elbow specimens

Figure 4.6 shows failure pressure for elbow assemblies, and it can be noted that there is a factor of 2.5 difference in the average of their failure pressure. A standard 2-tailed t-test, using a 95% confidence interval was performed on the data and indicates that drilled and eroded defects are statistically different from one another with a p-value of 0.011. Furthermore, the value for eroded defects is also lower than the theoretical prediction for this repair thickness. This indicates that erosion has a significant impact in the repair performance for elbows in terms of failure pressure. One possible explanation for this behavior is that the elliptical shape of the defect is causing a bending moment that

is pushing the steel in the opposite direction of the repair increasing the opening strains as seen in the FEA simulation.

4.2 Digital Image Correlation

To better understand the performance of repairs applied to the two defect types, DIC was performed on half of the tested specimens. In this section, out of plane displacements and strains in both hoop and axial directions were obtained. The relation between failure pressure and these strains measured at a given pressure is also explored. All values obtained were extracted in the defect area along a line in the axial direction as shown in Figure 4.7.

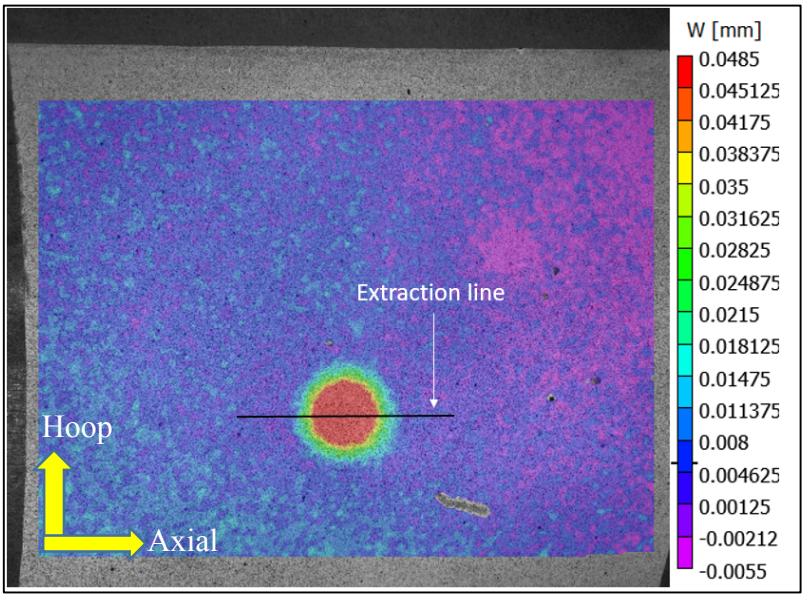

Figure 4.7: DIC extraction data line example

4.2.1 Straight Assembly with Two-Layer ply count

A total of 3 pipes were tested using this configuration. All pipes had a through-wall defect of 0.25 in diameter. Out of those 3 pipes, 1 had a drilled defect and 2 had eroded defects with elliptical shape with an extension of 11 times the diameter of the through-wall

defect in the axial directional and 6 times the diameter of the through-wall penetration in the hoop direction. All 3 pipes were tested at a pressure of 600 psi.

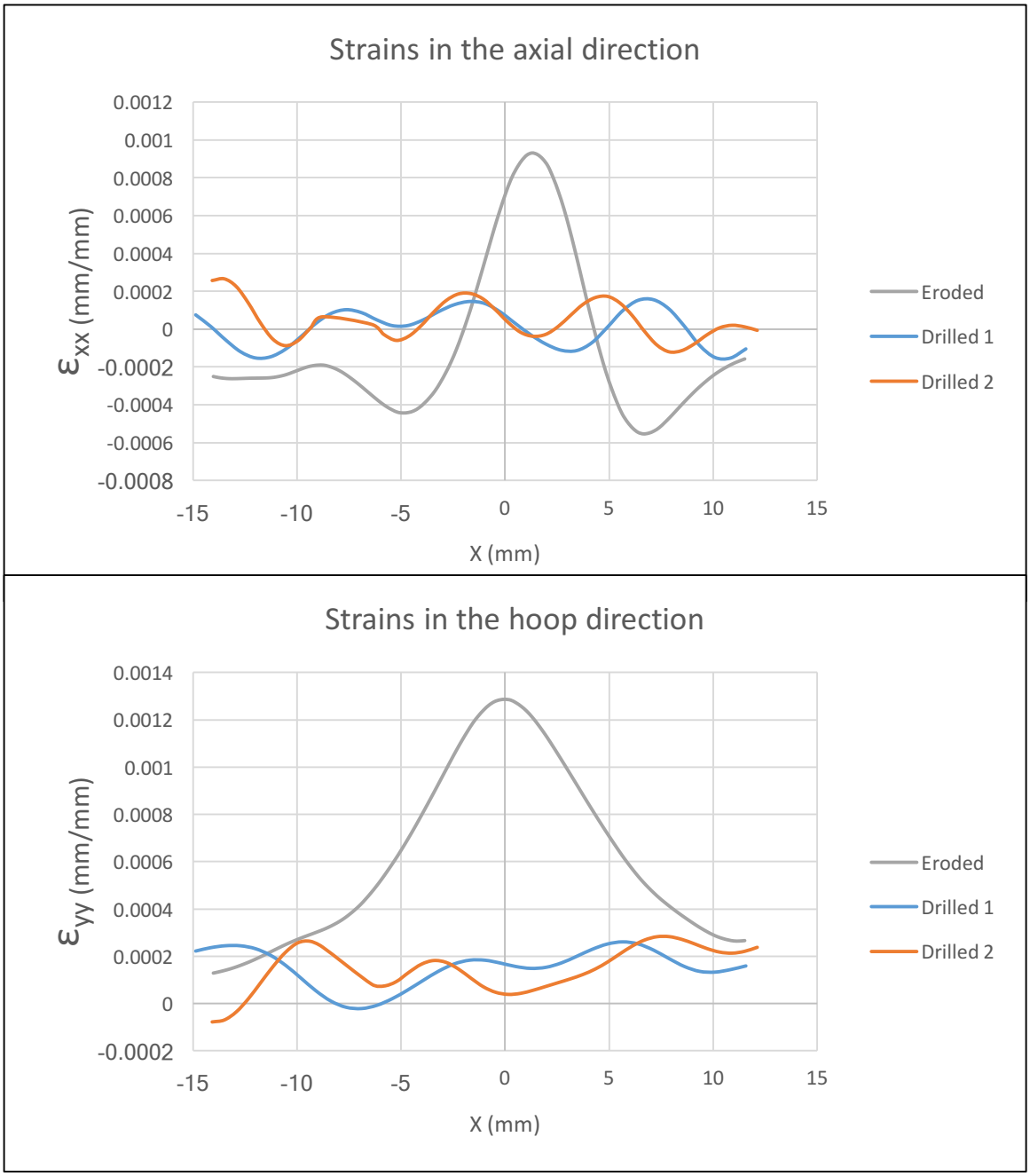

Figure 4.8: Hoop and axial strains for eroded and drilled defects with two-layer repair on straight specimens at 600 psi

Figure 4.8 shows a noticeable difference in strains in both directions between drilled and eroded defects.

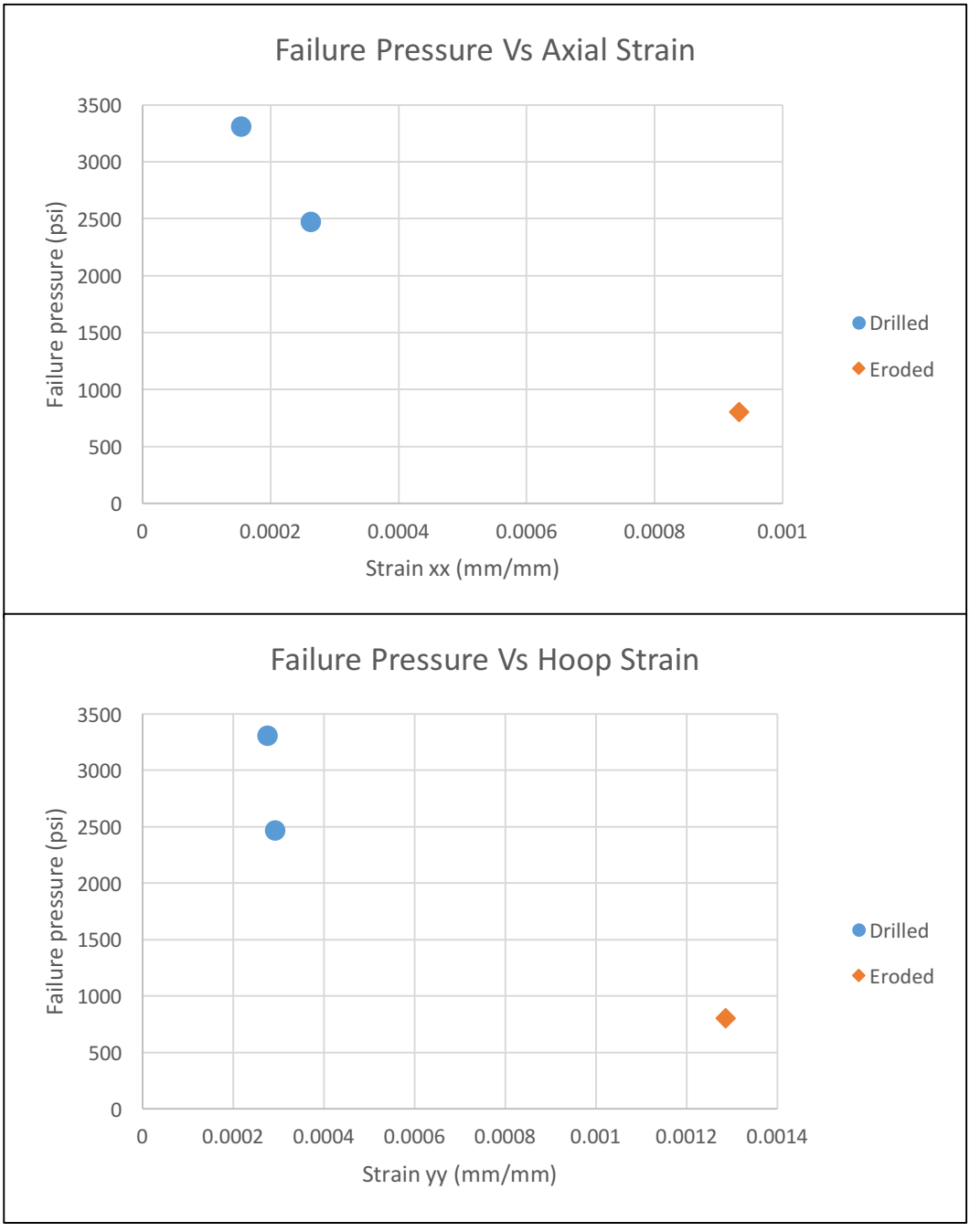

Figure 4.9: Failure pressure Vs strains obtained for eroded and drilled defects with two-layer repair on straight specimens at 600 psi

Figure 4.9 illustrates that these strains represent a big influence in the failure pressure of the specimens. Drilled defects with lower strains in both directions achieved higher failure pressures. This shows a very clear relation between strains and failure pressure. These higher strains may be achieved by the thin damage area deforming, and because this high deformation, they achieved lower failure pressure than for drilled defects.

4.2.2 Straight Assembly with Four-Layer ply count

A total of 6 pipes were tested with a four-layer repair on elbows. All pipes had a through-wall defect of 0.5 in diameter. Out of those 6 pipes, 3 had drilled defects and 3 had eroded defects. DIC was performed at a pressure of 800 psi.

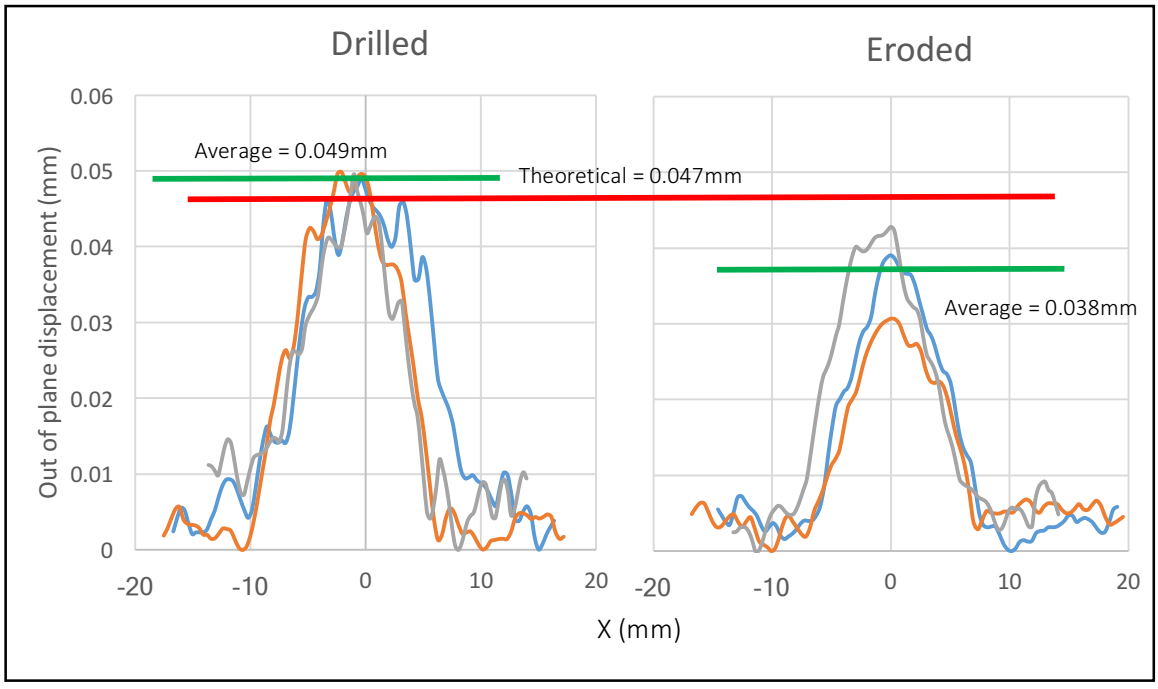

Figure 4.10: Out of plane displacement for eroded and drilled defects with two-layer repair on straight specimens at 800 psi

Figure 4.10 shows that the average of the maximum out of plane displacement for both defects is quite similar. Also, using Equation (2) from plate theory described in Section 1, measurements from both speciemns match well with the theoretical prediction for maximum displacement.

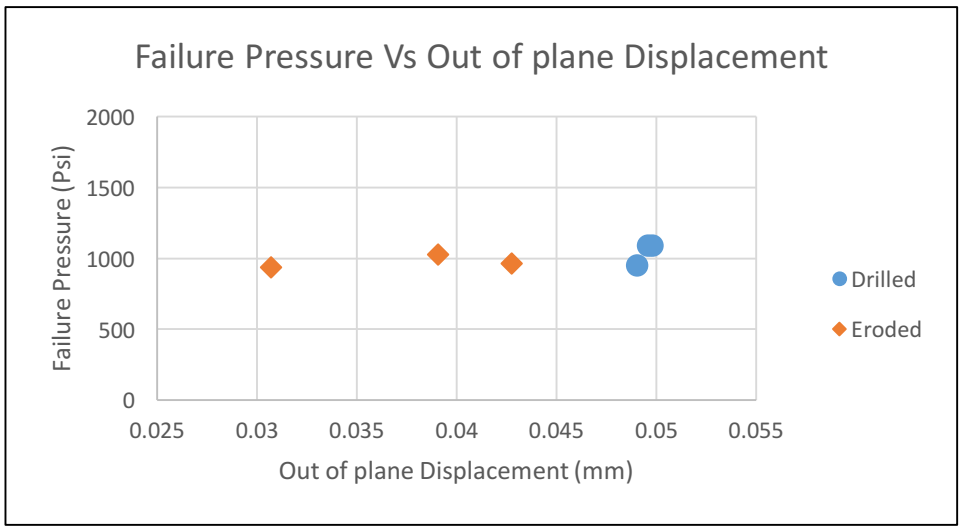

Figure 4.11: Failure pressure Vs out of plane displacement for eroded and drilled defects with four-layer repair on straight specimens at 800 psi

Figure 4.11 shows the maximum out of plane displacement vs. the failure pressure. The out of plane displacement appears to have little correlation to the failure pressure. This is probably because the difference in their averages for out of plane displacement is only 30%.

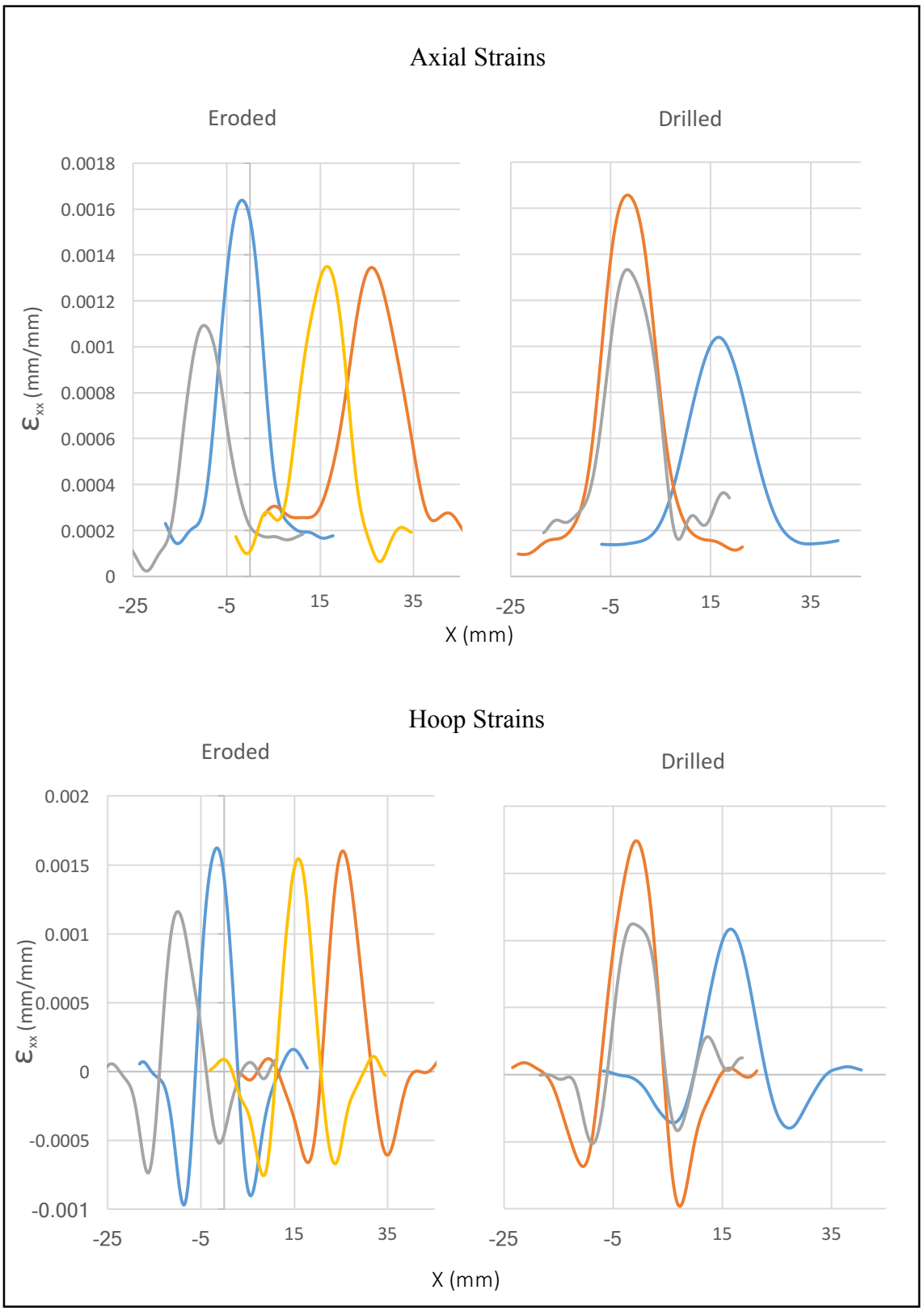

Figure 4.12: Strains in hoop and axial directions for eroded and drilled defects with four-layer repair on straight specimens at 800 psi

Both strains in the axial and in the hoop directions are very similar for both drilled and eroded defects as shown in Figure 4.12. The similarity between these two specimens is expected since the failure pressures are similar.

4.2.3 Elbow Assembly with Four-Layer Ply Count

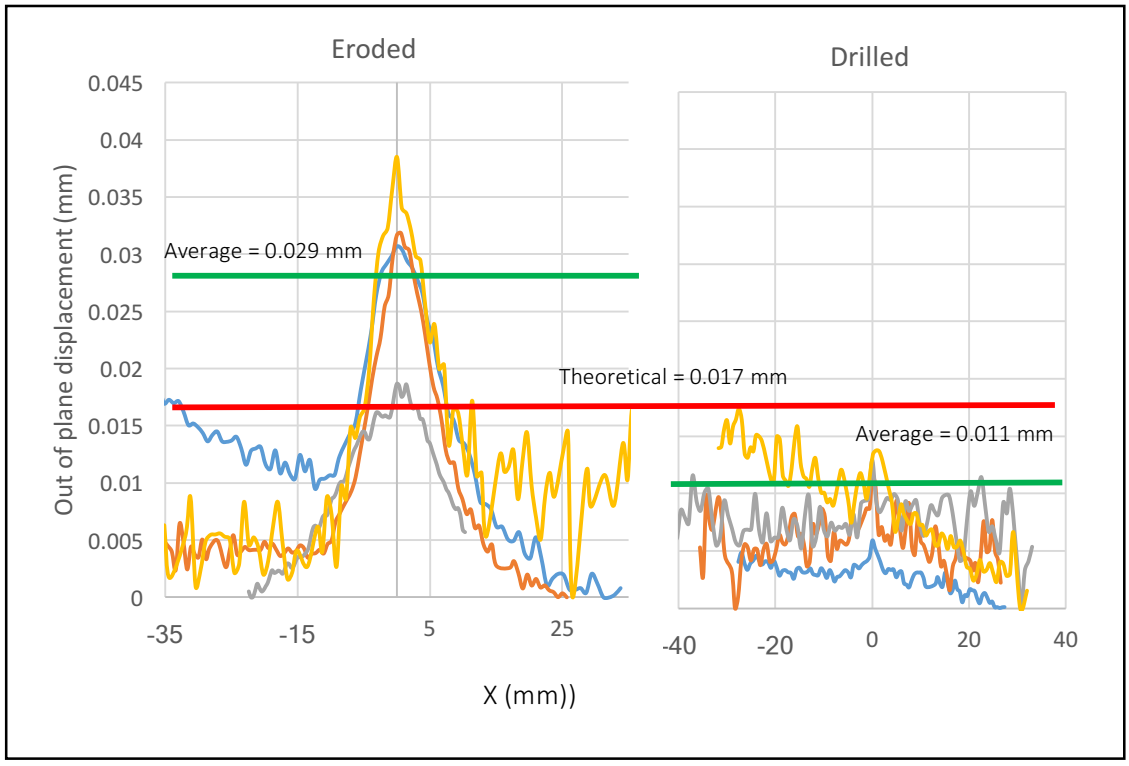

Figure 4.13 Out of plane displacement for eroded and drilled defects for four-layer repair on elbow assemblies at 1000 psi

A total of 9 elbow assemblies were tested using a four-layer repair. All pipes had a through-wall defect of 0.25 in diameter. Out of those 9 pipes, 4 had drilled defects and 5 had eroded defects with an eroded area having an elliptical shape with an extension diameter about 5 times bigger than the through-wall defect. Digital image correlation was performed at 1000 psi.

Figure 4.13 displays the difference in displacement for drilled and eroded defects in elbows. The maximum average displacement for eroded defects is 60% higher than theoretical prediction and almost three times the maximum average for drilled holes. This may be happening due to crack initiation sooner for eroded defects than for drilled ones.

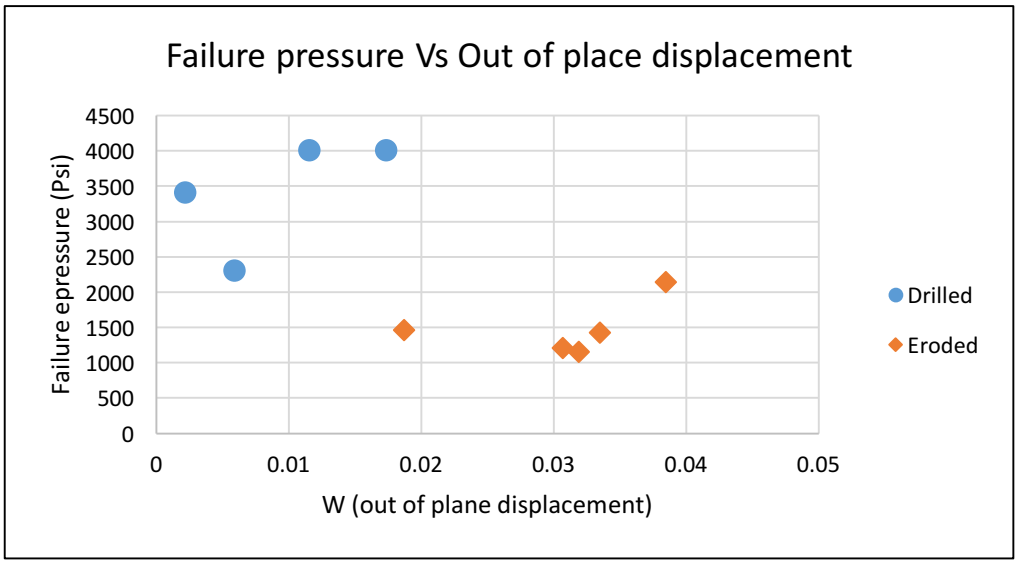

Figure 4.14: Failure pressure Vs out of plane displacement for eroded and drilled defects with four-layer repair on elbow assemblies at 1000 psi

Figure 4.14 shows the relation between failure pressure and out of plane displacement. It can be seen that for those specimens which the out of plane displacement is lower, failure pressure tends to be higher. However, there is one drilled and one eroded point which achieve about the same pressure having very different displacements. This is probably due to exceptional bond strength for the drilled sample having higher displacement or very high fracture toughness at the interface. However, further study is required to understand the performance difference at the extremes of failure pressure.

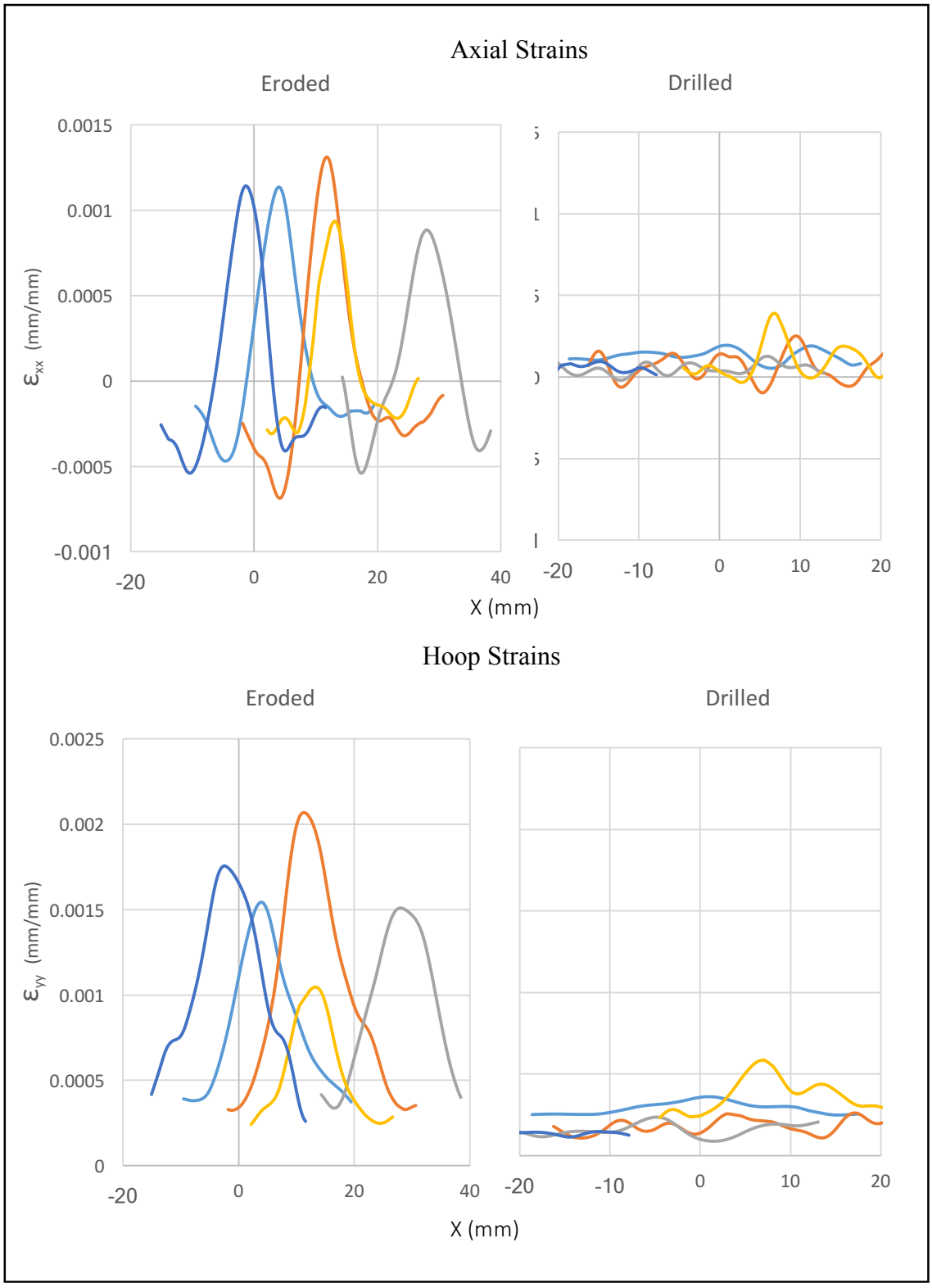

Figure 4.15: Strains in hoop and axial directions for eroded and drilled defects with four-layer repair on elbow specimens at 1000 psi

Figure 4.15 shows both strains in the axial and in the hoop directions are different for drilled and eroded defects. These specimens had the largest difference in failure pressures and this behavior is reflected in the strain behavior. Measured strains in the drilled specimens are extremely low when compared to the eroded specimens. This is expected based on the failure pressures.

4.3 FEA and DIC comparison

Several configurations of assemblies and ply count were compared to evaluate the accuracy of the FEA model. These combinations of assembly and ply count were selected to show a representative selection of all possible combinations of defects, assemblies, and repair thickness tested during the research.

4.3.1 Two-Layer Repair on Straight Specimen

The comparison shown in Figure 4.16 refers to the case for a two-layer repair on a straight specimen. In this case, the defect was modeled as an eroded defect with an elliptical eroded shape and the pressure was 700 psi. As observed below, theoretical and FEA match almost perfectly, and DIC results match very well following the clear trend for FEA and DIC.

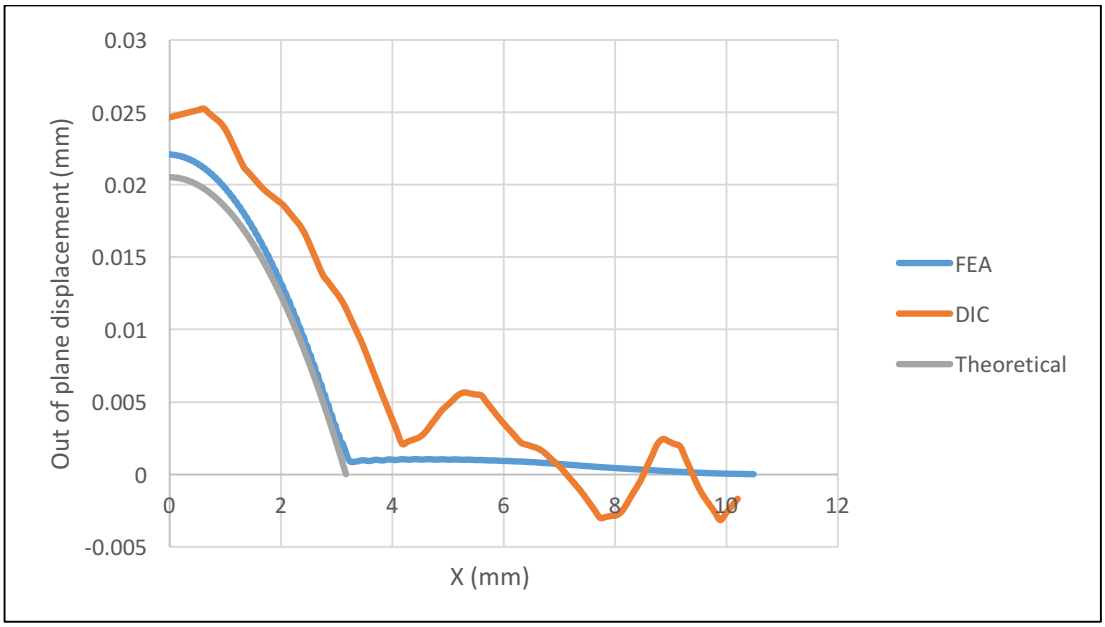

Figure 4.16: FEA and DIC Comparison. Out of plane displacement for two-layer repair on straight specimen

4.3.2 Four-Layer Repair on Straight Specimen

In this comparison, a drilled defect with 0.5 in diameter was simulated using a four-layer repair on a straight specimen. The pressure was 900 psi. This comparison will be made in terms of out of plane displacement and strains in both axial and hoop directions shown in Figures 4.17 to 4.19. The out of plane displacement shows the same trend as for two-layer repair, DIC is probably higher due to imperfections in the boding between the substrate and the repair because the FEA and theoretical approach consider this interface as perfectly bonded. It is also observed that the DIC curve starts at a different point from the theoretical and FEA curves. This is probably due to the fact that there is a crack growing at the interface between the repair and the substrate, so the repair starts deflecting beyond the edge of the through-wall defect.

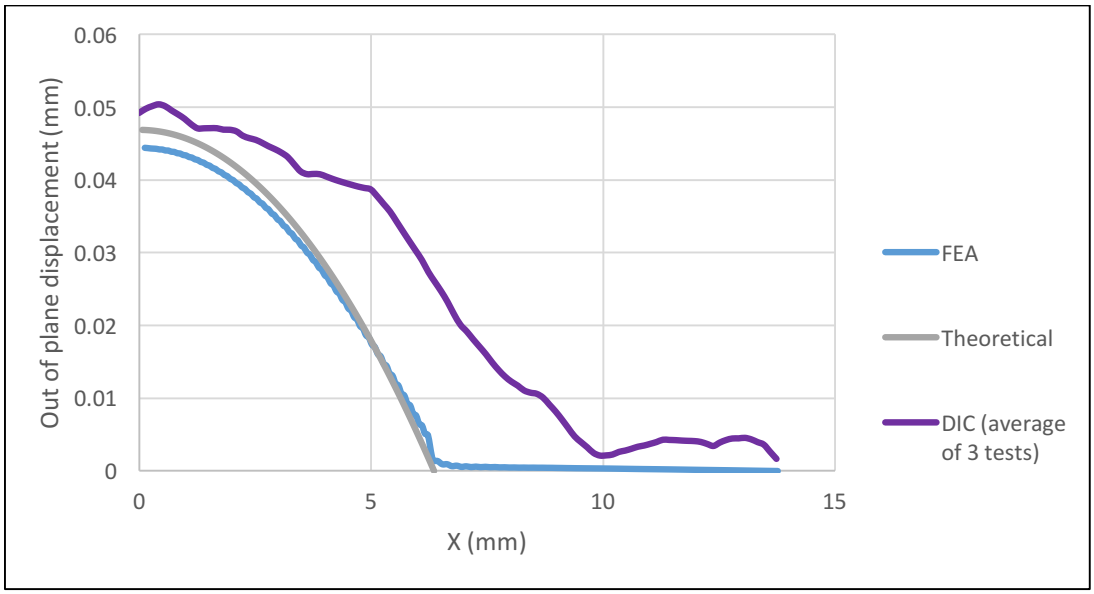

Figure 4.17: FEA and DIC Comparison. Out of plane displacement for four-layer repair on straight specimen

Figures 4.18 and 4.19 show comparison of strains in both hoop and axial directions. It is observed that DIC measurements agree well with FEA predictions. In both directions, the DIC measurements capture very well the trend of these strains.

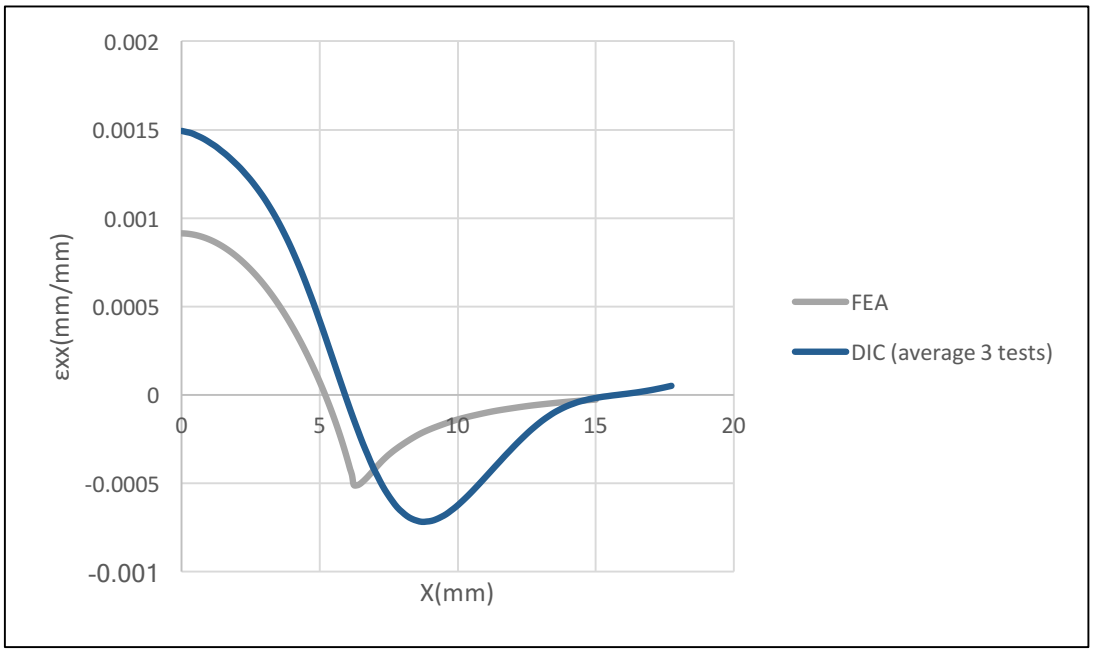

Figure 4.18: FEA and DIC Comparison. Axial strains for four-layer repair on straight specimen

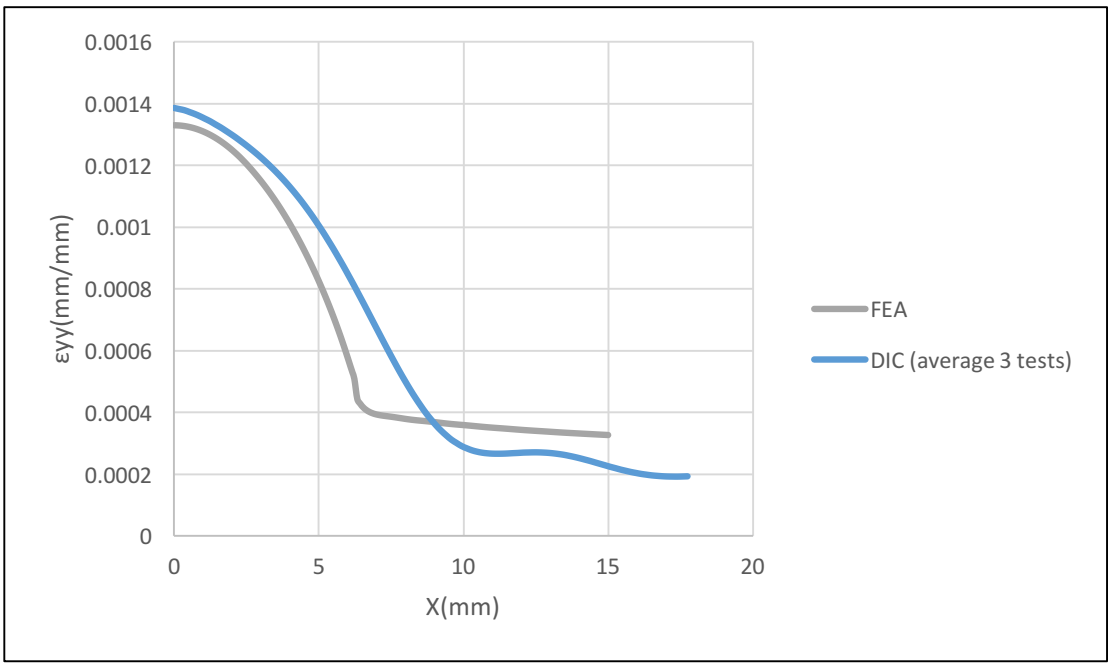

Figure 4.19: FEA and DIC Comparison. Hoop strains for four-layer repair on straight specimen

4.3.3 Four-Layer Repair on Elbow Specimen

Figure 4.20 shows the comparison of FEA, DIC, and theoretical contours for a four-layer repair on elbow specimen applied on an eroded defect at 1000 psi. As shown in both FEA and DIC, measurements of out of plane displacement were higher than the theoretical prediction for drilled defects. This is probably because the theoretical prediction does not take into account the thin wall of the substrate deforming along with the repair. Comparing FEA with DIC, both follow the same trend, but the magnitudes do not match as well as in the case of straight specimens with four-layer repair. Further studies are ongoing to determine the source of this mismatch.

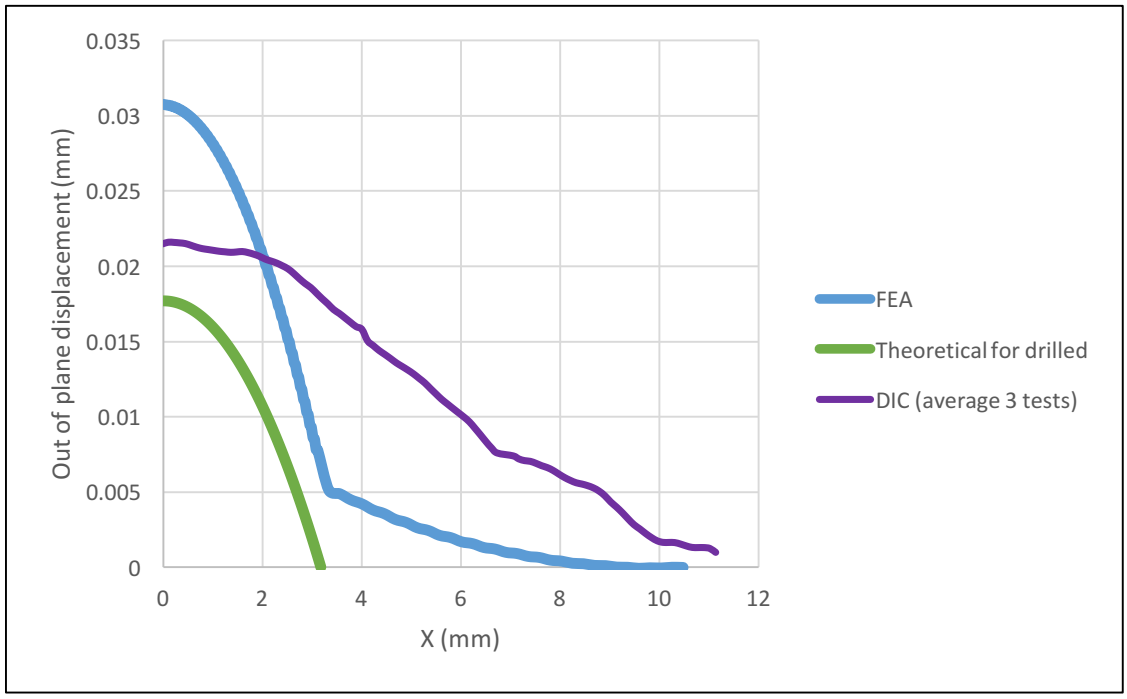

Figure 4.20: FEA and DIC Comparison. Out of plane displacement for four-layer repair on elbow specimen

5 CONCLUSIONS AND RECOMMENDATIONS

5.1 5.1 Conclusions

An experimental and FEA comparison was performed to determine the difference in performance of composite repairs on diffused and drilled defects in pipelines in terms of failure pressure, displacements and strains. Two geometries were used in this study, a straight pipe and an elbow. Also, two different thicknesses of repair were applied to the vessel: two and four layer. Two defects were generated on those pipes: drilled defects produced by simply drilling a hole on the substrate, and eroded defects which were generated using a dry erosion process using ground glass as blast media until the defect became a through-wall defect. After defects were created and specimens were assembled, they were repaired and hydrostatically tested. Simultaneously, Digital image correlation was performed in the defect region to obtain displacements and strains for every increment of pressure until failure.

For the FEA section, two studies were carried out in straight pipes investigating the impact of the size and shape of the eroded area. The goal of these studies were to understand how defected geometry affected the opening strains at the interface between the repair and the substrate. Opening strains at the interface are very important because these strain values indicate the likelihood of crack initiation and growth. In the size study, it was found that as the circular eroded area becomes larger, the strains decreased. This behavior indicates that strains decreased due to the thin wall of the substrate deforming outward with the

repair. Also, when the diameter of the eroded area approaches ten times the diameter of the hole, the strains remain almost constant. This indicates that erosion far from the defect does not have any impact in the performance of the repair. On the other hand, in the shape study, as the axial length of the ellipse became larger, the strains increased. One explanation for this behavior is that an elliptical eroded geometry creates a bending moment in which the region near the through-wall defect pushes in the opposite direction of the repair. This correlates with the experimental results in which the straight pipes having elliptical eroded defects showed this deformation in the region near the hole.

Furthermore, FEA was applied to elbow geometries to compare the opening strains at the interface for both defects. It was found that in the most critical section of the interface the strains were higher for the eroded defect. However, for the rest portion of the interface, the strains were higher for drilled defects. This may be occurring because, in the critical section, the substrate is moving in the opposite direction to the repair as seen before for elliptical defects on straight pipes.

Taking into consideration the failure pressure, eroded and drilled defects on straight specimens performed very similar for both two and four layer repair. This was true for eroded defects having a circular shape around the hole. However, for pipes having a two-layer repair and an elliptical eroded shape, the average failure pressure of drilled defects was about 4 times greater than for eroded defects. This tends to indicate that the shape of the erosion has a large impact on the repair performance. For the elbow assemblies, a difference of a factor of 2.5 was noted between drilled and eroded defects. Drilled defects possessed the highest failure pressure. These lower failure pressures achieved by elbows having eroded defects is probably due to the fact that elliptical eroded area creates a

bending moment causing the substrate in the region near the hole to deform in the opposite direction to the repair, making the crack initiate faster than for drilled defects.

In the case of strains and out of plane displacement, digital image correlation was performed to obtain the strains and displacements experimentally. Eroded and drilled defects on straight specimens had very close values for both two and four layer repairs. This correlates with the failure pressure since they achieved very similar failure pressures as well. For elbows, both axial and hoop strains were higher for the eroded defects when evaluated at the pressure of 1000 psi. This has a direct relation with the failure pressure, since for drilled defects which had lower strains, the specimens achieved a higher failure pressure.

When comparing digital image correlation with FEA results for strains and displacements, it was observed that both the trend and the values match well for the straight specimens. In the case of out of plane displacements for elbows, the trend is very similar but the values do not match very well. This is probably due to imperfections in the repair such as voids or installation errors.

5.2 Recommendations

For composite repairs installed on through-wall defects, or defects that may become through wall, the symmetry of the diffuse damage region appears to be the most significant determining factor. If symmetry of the underlying damage can be assumed, then the existing design methodology for through-wall repairs is likely sufficient for a conservative repair design. For the case of non-symmetric or elliptical damage, the existing design methodology appears to be non-conservative. For the case of significant ellipticity, even if the through-wall penetration is circular, the use of the axial flaw equations in PCC2 is

recommended. Adopting this design methodology appears to produce a conservative design in these cases.

While this study has provided an important first step in understanding diffuse damage, there are some more experiments and simulations that should be pursued to develop a more complete understanding of repair behavior. For example, larger damaged areas should be generated on both elbow and straight specimens to understand if the FEA-predicted behavior is accurate. Additionally, different types of assemblies should be tested. A tee specimen is recommended in further studies because it is a common structure found in the field. These tests will provide a better idea of the severity of these defects for different assemblies in the repair performance.

BIBLIOGRAPHY

[1] Wood, R. J. K., Jones, T. F., Miles, N. J., & Ganeshalingam, J. (2001). "Upstream swirl-induction for reduction of erosion damage from slurries in pipeline bends". Wear, 250(1), 770-778

[2] Shirazi, S. A., Shadley, J. R., McLaury, B. S., & Rybicki, E. F. (1995). "A procedure to predict solid particle erosion in elbows and tees". Journal of Pressure Vessel Technology, 117(1), 45-52.

[3] Ukpai, J. I., Barker, R., Hu, X., & Neville, A. (2013). "Exploring the erosive wear of X65 carbon steel by acoustic emission method". Wear, 301(1), 370-382.

[4] Malka, R., Nešić, S., & Gulino, D. A. (2007). "Erosion–corrosion and synergistic effects in disturbed liquid-particle flow". Wear, 262(7), 791-799.

[5] Hu, X., & Neville, A. (2009). "CO 2 erosion–corrosion of pipeline steel (API X65) in oil and gas conditions—a systematic approach". Wear, 267(11), 2027-2032.

[6] Islam, M. A., & Farhat, Z. N. (2014). "Effect of impact angle and velocity on erosion of API X42 pipeline steel under high abrasive feed rate". Wear,311(1), 180-190

[7] Andrews, D. The erosion of metals. University of Cambridge 1980.

[8] Bellman, R. and Levy, A., 1981. “Erosion mechanism in ductile metals”. Wear, 70(1), pp.1-27.

[9] Mableson R, Patrick C, Dodds N, Gibson G. “Refurbishment of steel tubulars using composite materials”. Plast Rubber. Compos 2000; 29 (10):558–65.

[10] Greenwood C., 2001. “Composite pipe repair method shows versatility, long-lasting”. Pipeline and Gas Journal, 228(2), pp.58-58

[11] Costs, C. (2002). Preventive Strategies in the United States, Publication No. FHWA-RD-01-156, as found in Supplement to Materials Performance.

[12] K. Farrag, “Selection of pipe repair methods,” Final report GTI project number 21087, Gas Technology Institute, 2013.

[13] Alexander, C. “Advances in the repair of pipelines using composite materials"**.** Stress Engineering Services, Inc.

[14] Wilson, J. “Characterization of a Carbon Fiber Reinforced Polymer Repair System for Structurally Deficient Steel Piping”. University of Tulsa 2006.

[15] ASME, "Post Construction Code," in Nonmetallic and Bonded Repairs. New York: ASME, 2011.

[16] J. M. Duell, “Characterization and FEA of a carbon composite overwrap repair system,” University of Tulsa, 2004.

[17] P. Smith and J. Cuthill, “Patching up pipework with carbon-fiber composites,” Mater World, vol. 10, no. 5, p. 28, 2002.

[18] Mazumder, Q.H., 2012. “Effect of liquid and gas velocities on magnitude and location of maximum erosion in U-bend”. Open Journal of Fluid Dynamics, vol. 2, No. 2, 2012

[19] Edwards, J.K., McLaury, B.S. and Shirazi, S.A., 2001. “Modeling solid particle erosion in elbows and plugged tees”. Journal of Energy Resources Technology, 123(4), pp.277-284.

[20] Levy, A.V. and Chik, P., 1983. “The effects of erodent composition and shape on the erosion of steel”. Wear, 89(2), pp.151-162.